AN ABSTRACT OF THE THESIS OF

Leonard C. Hainz III for the degree of Master of Science in Mechanical Engineering presented on August 20, 2004.

Title: Modified Linear Theory and Kalman Filtering for In Flight Projectile Impact Point Prediction.

Abstract approved: Redacted for privacy

Mark F. Costello

A method for real time in-flight prediction of the ground impact point of an indirect fire projectile is investigated. The method investigated is comprised of a combination of an impact point predictor and an extended Kalman filter state estimator based on modified linear theory. The modified linear theory model is formed through a re-derivation of projectile linear theory with a less restrictive set of assumptions. Performance documentation for the modified linear theory model is provided in the form of typical results for both a short range trajectory of a direct fire fin stabilized projectile and a long range trajectory for an indirect fire spin stabilized round. The extended Kalman filter blends sensor data with an internal modified linear theory model to obtain an estimate of the projectile state. Three sensor configurations are explored, each assuming that sensor measurements are available at discrete times during flight. Results generated from a previously validated non-linear six degree of freedom projectile model and simulated noisy sensor readings indicate the technique is capable of predicting ground impact to within 15 meters at the apex of the trajectory when full state feedback is available.

Modified Linear Theory and Kalman Filtering for In Flight Projectile Impact Point Prediction

by

Leonard C. Hainz III

A THESIS

submitted to

Oregon State University

in partial fulfillment of

the requirements for the

degree of

Master of Science

Presented August 20, 2004

Commencement June 2005

Master of Science thesis of Leonard C. Hainz III presented on August 20, 2004.

APPROVED:

Redacted for privacy

Major Professor, representing Mechanical Engineering

Redacted for privacy

Head of the Department of Mechanical Engineering

Redacted for privacy

Dean of the Graduate School

I understand that my thesis will become part of the permanent collection of Oregon State University libraries. My signature below authorizes release of my thesis to any reader upon request.

Redacted for privacy

Leonard C. Hainz III, Author

TABLE OF CONTENTS

TABLE OF CONTENTS (Continued)

LIST OF FIGURES

LIST OF FIGURES (Continued)

GENERAL INTRODUCTION

Many powerful smart weapon control techniques rely on accurate observation of the full projectile state. The use of on-board sensors for projectile state observation is plagued by the noise inherent in physical sensors while the use of on-board state propagators is plagued by inaccuracies inherent in simple dynamic models. The two papers comprising this thesis outline a complete impact point estimation algorithm. The first paper proposes a modified projectile linear theory model that significantly improves accuracy of state propagation while still maintaining the low computation overhead required for real time implementation of a smart weapon control law. The second paper considers the combination of an extended Kalman filter based on modified linear theory and a propagator for impact point estimation.

MODIFIED PROJECTILE LINEAR THEORY FOR RAPID TRAJECTORY PREDICTION

Leonard C. Hainz III and Mark Costello

AIAA Journal of Guidance, Control, and Dynamics

1801 Alexander Bell Drive, Suite 500

Reston, VA 20191-4344

Submitted, In review as of 9/2004

ABSTRACT

In some smart weapons estimation of the impact point of the shell at each computation cycle of the control law is an integral part of the control strategy. Since the impact point predictor is part of the imbedded computing system onboard the projectile, practical considerations dictate that the impact point predictor yield rapid yet reasonably accurate estimates. The two most common methods for rapid trajectory prediction are numerical integration of the point mass dynamic equations and evaluation of the closed form solution of the rigid body projectile dynamic equations produced by standard projectile linear theory. These methods are shown to exhibit poor impact point prediction for long range shots with high gun elevations characteristic of smart indirect fire munitions. Through modifications of projectile linear theory, a rapid projectile impact point predictor is proposed that eliminates the accuracy problems of the other methods while preserving low computational requirements. Typical results are provided for a short range trajectory of a direct fire fin stabilized projectile and a long range trajectory for an indirect fire spin stabilized round to substantiate these claims.

NOMENCLATURE

A, B, C, E	epicyclic matrix coefficients
a_V, b_V	velocity solution coefficients
C_{DD}	roll moment aerodynamic coefficient due to fin cant
C_{LP}	roll damping aerodynamic coefficient

C_{MQ}	pitch damping aerodynamic coefficient
C_{NA}	normal force aerodynamic coefficient
C_{NPA}	Magnus force aerodynamic coefficient
C_{NR}	yaw damping aerodynamic coefficient
C_{X0}	zero yaw axial force aerodynamic coefficient
C_{X2}	yaw angle squared axial force aerodynamic coefficient
C_{Y0}	trim side force aerodynamic coefficient
C_{YB1}	normal force aerodynamic coefficient along j_n axis
C_{Z0}	trim vertical force aerodynamic coefficient
C_{ZA1}	normal force aerodynamic coefficient along k_{nr} axis
D	projectile reference diameter
F_v, F_w, F_q, F_r	epicyclic equations forcing coefficients
g	gravity
I	projectile inertia matrix
I_{XX}, I_{YY}, I_{ZZ}	diagonal components of the inertia matrix
I_{XY}, I_{YZ}, I_{XZ}	off-diagonal components of the inertia matrix
$\tilde{L}, \tilde{M}, \tilde{N}$	external moments on projectile, expressed in the no-roll frame
$\tilde{L}_A, \tilde{M}_A, \tilde{N}_A$	moment due to aerodynamic force, expressed in the no-roll frame
$\tilde{L}_M, \tilde{M}_M, \tilde{N}_M$	moment due to Magnus force, expressed in the no-roll frame

$\widetilde{L}_{UA}, \widetilde{M}_{UA}, \widetilde{N}_{UA}$	unsteady aerodynamic moment, expressed in the no-roll frame
m	mass of projectile
$\widetilde{p}$	projectile roll rate, expressed in no-roll frame
$\widetilde{q}, \widetilde{r}$	projectile pitch and yaw rates, expressed in the no-roll frame
$R_{\oplus CA}$	vector from the projectile center of mass to the center of pressure
$R_{\oplus CM}$	vector from the projectile center of mass to the Magnus center of pressure
R_{MCM}	distance from center of mass to Magnus center of pressure along station line
R_{MCP}	distance from center of mass to center of pressure along station line
s	dimensionless arc length
t	time
T_{NRI}	transformation matrix from no-roll frame to inertial frame
$\widetilde{u}, \widetilde{v}, \widetilde{w}$	projectile velocity components, expressed in no-roll frame
$\widetilde{u}_A, \widetilde{v}_A, \widetilde{w}_A$	projectile aerodynamic velocity components, expressed in the no-roll frame
$\widetilde{u}_W, \widetilde{v}_W, \widetilde{w}_W$	wind velocity, expressed in the no-roll frame
V	Total velocity
V_A	Total aerodynamic velocity
x, y, z	projectile position in inertial space
$\widetilde{X}, \widetilde{Y}, \widetilde{Z}$	external forces on projectile expressed in the no-roll frame
$\widetilde{X}_A, \widetilde{Y}_A, \widetilde{Z}_A$	aerodynamic force acting on the projectile expressed in the no-roll frame
$\widetilde{X}_M, \widetilde{Y}_M, \widetilde{Z}_M$	Magnus force acting on the projectile expressed in the no-roll frame

$\tilde{X}_w, \tilde{Y}_w, \tilde{Z}_w$	weight force acting on the projectile expressed in the no-roll frame
α, β	Aerodynamic angles of attack
ϕ	projectile roll angle
θ, ψ	projectile pitch and yaw angles
ρ	atmospheric density
Φ_F, Φ_S	epicyclic Eigen value imaginary components
σ_F, σ_S	epicyclic Eigen value real components

INTRODUCTION

Over 80 years ago, pioneering English ballisticians Fowler, Gallop, Lock, and Richmond constructed the first rigid 6 degree of freedom projectile exterior ballistics model [1]. Their model contained a reasonably complete aerodynamic force and moment expansion for a spinning shell and included aerodynamic damping along with Magnus force and moment. Guided by an extensive set of yaw card firings, these researchers also created the first approximate analytic solution of the 6 degree of freedom projectile equations of motion by introducing a set of simplifications based on the relative size of different dynamic quantities of a stable projectile and based on clever linearization by artificially separating the dynamic equations into uncoupled groups. The resulting theory is commonly called projectile linear theory. Refinements and improvements to projectile linear theory were made by Kent [2], Neilson and Synge [3], and Kelly and McShane [4, 5]. Projectile linear theory has proved an invaluable tool in understanding basic dynamic characteristics of projectiles in atmospheric flight, for establishing stability criteria for fin

and spin stabilized projectiles, and for extracting projectile aerodynamic loads from spark range data. Various authors have extended projectile linear theory to accommodate asymmetric mass properties [6], fluid payloads [7, 8], moving internal parts [9, 10, 11], ascending flight [12], lateral force impulses [13, 14], and dual-spin projectiles [15, 16].

For the design of some smart weapon flight control systems, prediction of the impact point during flight is an integral part of the control law [17]. While projectile linear theory provides qualitatively correct trajectories, impact point prediction errors are relatively large, particularly for high launch angles and long range trajectories. The work reported here documents several modifications to standard projectile linear theory that significantly improve accuracy of impact point prediction while still maintaining low computation overhead required for real time implementation of a smart weapon control law.

PROJECTILE DYNAMIC MODEL

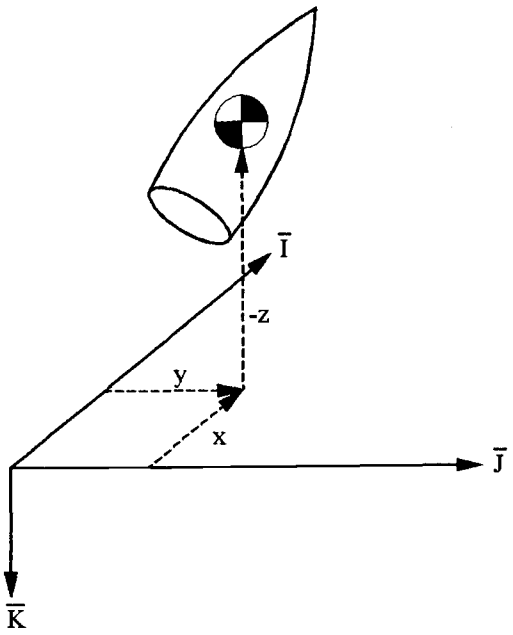

Figure 1.1: Projectile Position Coordinate Definitions

A six-degree of freedom rigid projectile model is employed to predict the dynamics of a projectile in flight. The six degrees of freedom are comprised of the three translational components describing the position of the projectile's center of mass, and the three Euler angles describing the orientation of the projectile with respect to a fixed inertial axis. Figures 1.1 and 1.2 provide a visualization of the degrees of freedom. The equations of motion for the six-degree of freedom model, derived in the no-roll frame, are shown in equations (1-4).

$$\begin{Bmatrix} \dot{x} \\ \dot{y} \\ \dot{z} \end{Bmatrix} = \begin{bmatrix} c_\theta c_\psi & -s_\psi & s_\theta c_\psi \\ c_\theta s_\psi & c_\psi & s_\theta s_\psi \\ -s_\theta & 0 & c_\theta \end{bmatrix} \begin{Bmatrix} \tilde{u} \\ \tilde{v} \\ \tilde{w} \end{Bmatrix} \tag{1}$$

$$\begin{Bmatrix} \dot{\phi} \\ \dot{\theta} \\ \dot{\psi} \end{Bmatrix} = \begin{bmatrix} 1 & 0 & t_\theta \\ 0 & 1 & 0 \\ 0 & 0 & 1/c_\theta \end{bmatrix} \begin{Bmatrix} \tilde{p} \\ \tilde{q} \\ \tilde{r} \end{Bmatrix} \tag{2}$$

$$\begin{Bmatrix} \dot{\tilde{u}} \\ \dot{\tilde{v}} \\ \dot{\tilde{w}} \end{Bmatrix} = \begin{Bmatrix} \tilde{X}/m \\ \tilde{Y}/m \\ \tilde{Z}/m \end{Bmatrix} + \begin{Bmatrix} \tilde{r}\tilde{v} - \tilde{q}\tilde{w} \\ -t_\theta \tilde{r}\tilde{w} - \tilde{r}\tilde{u} \\ \tilde{q}\tilde{u} + t_\theta \tilde{r}\tilde{v} \end{Bmatrix} \tag{3}$$

$$\begin{Bmatrix} \dot{\tilde{p}} \\ \dot{\tilde{q}} \\ \dot{\tilde{r}} \end{Bmatrix} = [I]^{-1} \left(\begin{Bmatrix} \tilde{L} \\ \tilde{M} \\ \tilde{N} \end{Bmatrix} + \begin{bmatrix} 0 & -\tilde{r} & \tilde{q} \\ \tilde{r} & 0 & \tilde{r}t_\theta \\ -\tilde{q} & -\tilde{r}t_\theta & 0 \end{bmatrix} [I] \begin{Bmatrix} \tilde{p} \\ \tilde{q} \\ \tilde{r} \end{Bmatrix} \right) \tag{4}$$

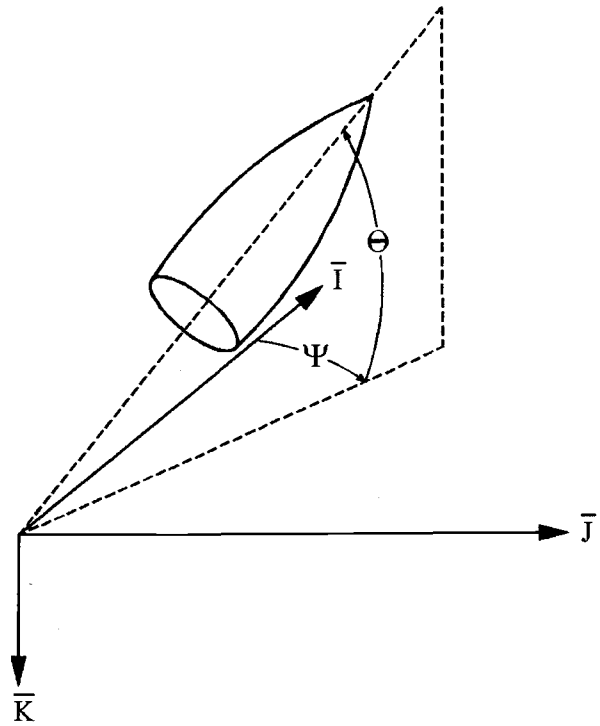

Figure 1.2: Projectile Orientation Definitions

The force acting on the projectile in equation (3) is comprised of the weight force (W) and the aerodynamic force. The aerodynamic force is split into a standard (A) and Magnus (M) aerodynamic force. The combination of forces is expressed in equations (5).

$$\begin{Bmatrix} \tilde{X} \\ \tilde{Y} \\ \tilde{Z} \end{Bmatrix} = \begin{Bmatrix} \tilde{X}_w \\ \tilde{Y}_w \\ \tilde{Z}_w \end{Bmatrix} + \begin{Bmatrix} \tilde{X}_A \\ \tilde{Y}_A \\ \tilde{Z}_A \end{Bmatrix} + \begin{Bmatrix} \tilde{X}_M \\ \tilde{Y}_M \\ \tilde{Z}_M \end{Bmatrix} \tag{5}$$

Equation (6) provides the expression for the weight force in the no-roll coordinate system.

$$\begin{Bmatrix} \tilde{X}_w \\ \tilde{Y}_w \\ \tilde{Z}_w \end{Bmatrix} = mg \begin{Bmatrix} -s_\theta \\ 0 \\ c_\theta \end{Bmatrix} \tag{6}$$

Equation (7) provides the expression for the aerodynamic force in the no-roll coordinate system. This force acts upon the projectile at the aerodynamic center of pressure.

$$\begin{Bmatrix} \tilde{X}_A \\ \tilde{Y}_A \\ \tilde{Z}_A \end{Bmatrix} = -\frac{\pi}{8}\rho {V_A}^2 D^2 \begin{Bmatrix} C_{X0} + C_{X2}\alpha^2 + C_{X2}\beta^2 \\ C_{Y0} + C_{YB1}\beta \\ C_{Z0} + C_{ZA1}\alpha \end{Bmatrix} \tag{7}$$

Equation (8) provides the expression for the Magnus force in the no-roll coordinate system. The Magnus force acts upon the projectile at the Magnus force center of pressure.

$$\begin{Bmatrix} \tilde{X}_M \\ \tilde{Y}_M \\ \tilde{Z}_M \end{Bmatrix} = \frac{\pi}{8}\rho {V_A}^2 D^2 \begin{Bmatrix} 0 \\ \dfrac{\tilde{p}DC_{NPA}\alpha}{2V_A} \\ \dfrac{-\tilde{p}DC_{NPA}\beta}{2V_A} \end{Bmatrix} \tag{8}$$

Equations (7-8) are based on Mach number dependent coefficients, the aerodynamic angles of attack given in equations (9-10), and the total aerodynamic velocity given in equation (11).

$$\alpha = \tan^{-1}\left(\widetilde{w}_A/\widetilde{u}_A\right) \tag{9}$$

$$\beta = \tan^{-1}\left(\widetilde{v}_A/\widetilde{u}_A\right) \tag{10}$$

$$V_A = \sqrt{\widetilde{u}_A^{\,2} + \widetilde{v}_A^{\,2} + \widetilde{w}_A^{\,2}} \tag{11}$$

The moment acting on the projectile in equation (4) is comprised of the moment due to the standard aerodynamic force (A), the moment due to the Magnus aerodynamic force (M), and the unsteady aerodynamic moment (UA) as shown in equation (12).

$$\begin{Bmatrix} \widetilde{L} \\ \widetilde{M} \\ \widetilde{N} \end{Bmatrix} = \begin{Bmatrix} \widetilde{L}_A \\ \widetilde{M}_A \\ \widetilde{N}_A \end{Bmatrix} + \begin{Bmatrix} \widetilde{L}_M \\ \widetilde{M}_M \\ \widetilde{N}_M \end{Bmatrix} + \begin{Bmatrix} \widetilde{L}_{UA} \\ \widetilde{M}_{UA} \\ \widetilde{N}_{UA} \end{Bmatrix} \tag{12}$$

The moment due to the aerodynamic force is expressed in equation (13).

$$\begin{Bmatrix} \tilde{L}_A \\ \tilde{M}_A \\ \tilde{N}_A \end{Bmatrix} = \begin{bmatrix} 0 & -R_{\oplus CAZ} & R_{\oplus CAY} \\ R_{\oplus CAZ} & 0 & -R_{\oplus CAX} \\ -R_{\oplus CAY} & R_{\oplus CAX} & 0 \end{bmatrix} \begin{Bmatrix} \tilde{X}_A \\ \tilde{Y}_A \\ \tilde{Z}_A \end{Bmatrix} \tag{13}$$

The moment due to the Magnus force is expressed in equation (14).

$$\begin{Bmatrix} \tilde{L}_M \\ \tilde{M}_M \\ \tilde{N}_M \end{Bmatrix} = \begin{bmatrix} 0 & -R_{\oplus CMZ} & R_{\oplus CMY} \\ R_{\oplus CMZ} & 0 & -R_{\oplus CMX} \\ -R_{\oplus CMY} & R_{\oplus CMX} & 0 \end{bmatrix} \begin{Bmatrix} \tilde{X}_M \\ \tilde{Y}_M \\ \tilde{Z}_M \end{Bmatrix} \tag{14}$$

The unsteady aerodynamic moments acting on the projectile are expressed in equation (15).

$$\begin{Bmatrix} \tilde{L}_{UA} \\ \tilde{M}_{UA} \\ \tilde{N}_{UA} \end{Bmatrix} = \frac{\pi}{8}\rho V_A^{\,2} D^3 \begin{Bmatrix} C_{DD} + \dfrac{\tilde{p}DC_{LP}}{2V_A} \\ \dfrac{\tilde{q}DC_{MQ}}{2V_A} \\ \dfrac{\tilde{r}DC_{NR}}{2V_A} \end{Bmatrix} \tag{15}$$

The coefficients used in this model are projectile specific functions of the Mach number of the projectile. The dynamic equations of motion expressed in equations (1-15) are highly nonlinear. Due to this fact, numerical integration is commonly used to obtain solutions to this initial value problem.

MODIFIED PROJECTILE LINEAR THEORY

Mathematically, the projectile dynamic model discussed above consists of 12 highly nonlinear ordinary differential equations. These equations are not amenable to a closed form solution. Simplifications to the dynamic equations have been identified over time, which yield an analytically solvable set of quasi-linear differential equations that enable rapid trajectory construction. Projectile linear theory provides reasonably accurate trajectory prediction for flat fire short trajectories. For high quadrant elevation shots or long distance trajectories, qualitatively correct trajectories are generated. However, in these cases significantly impact point prediction errors are noticed with conventional projectile linear theory. In order to improve trajectory prediction, the solution procedure is altered and the typical assumption of small Euler pitch angle is relaxed. To develop the projectile linear theory equations, the following set of simplifications are employed:

(1) The station line velocity ($\tilde{u}$), roll rate ($\tilde{p}$), and roll angle (ϕ) are large in relation to the side velocities ($\tilde{v}$ and $\tilde{w}$), yaw angle (ψ), pitch and yaw rates ($\tilde{q}$ and $\tilde{r}$), and wind velocity components ($\tilde{u}_W, \tilde{v}_W, \tilde{w}_W$). Products of small values and derivatives of small values are treated as negligible.

(2) The yaw angle (ψ) is small, allowing the simplifications expressed in equation (16) to hold.

$$\sin(\psi) \approx \psi \qquad \cos(\psi) \approx 1 \tag{16}$$

(3) The aerodynamic angles of attack are also small in magnitude, allowing the angles of attack to be expressed by equations (17-18) instead of equations (9-10).

$$\alpha \approx \tilde{w}/V \tag{17}$$

$$\beta \approx \tilde{v}/V \tag{18}$$

(4) The Magnus force components are small in comparison with the weight and aerodynamic force components so they are treated as negligible in the modified linear theory force computations. The Magnus force does create a non-negligible moment, so it is maintained in the moment computations.

(5) The projectile is geometrically symmetrical about the station line. This allows the inertia matrix to be simplified as shown in equations (19-20).

$$I_{XY} = I_{YZ} = I_{XZ} = 0 \tag{19}$$

$$I_{YY} = I_{ZZ} \tag{20}$$

(6) The projectile is aerodynamically symmetric. This allows the aerodynamic coefficients to be simplified as expressed in equations (21-23). This also allows for a

simplification in the expressions of the distances from the center of mass to both the standard aerodynamic and Magnus centers of pressure as expressed in equation (24.)

$$C_{MQ} = C_{NR} \tag{21}$$

$$C_{Y0} = C_{Z0} = 0 \tag{22}$$

$$C_{YB1} = C_{ZB1} = C_{NA} \tag{23}$$

$$\begin{aligned} R_{\oplus CAX} &= R_{MCP} & \qquad R_{\oplus CMX} &= R_{MCM} \\ R_{\oplus CAY} &= R_{\oplus CAZ} = 0 & \qquad R_{\oplus CMY} &= R_{\oplus CMZ} = 0 \end{aligned} \tag{24}$$

(7) The wind velocity component ($\tilde{u}_W$) parallel to the projectile station line is negligible in comparison to the projectile total velocity.

(8) A change of variables is introduced in which the station line velocity ($\tilde{u}$) is replaced by the projectile total velocity (V). Equation (25) expresses the projectile total velocity, and the application of assumption (1). Equation (26) expresses the time derivative of the total velocity, and the application of assumption (1).

$$V = \sqrt{\tilde{u}^2 + \tilde{v}^2 + \tilde{w}^2} \approx \tilde{u} \tag{25}$$

$$\dot{V} = \left(\tilde{u}\dot{\tilde{u}} + \tilde{v}\dot{\tilde{v}} + \tilde{w}\dot{\tilde{w}}\right)/V \approx \dot{\tilde{u}} \tag{26}$$

(9) Another change of variables is performed to convert the independent variable from time, t, to dimensionless arc-length, s. The arc-length, defined in equation (28), is dimensionless and expresses the projectiles downrange travel in calibers.

$$s = \frac{1}{D}\int_0^t V d\tau \tag{27}$$

Equations (29-30) express the relationships between time derivatives and arc-length derivatives in terms of an example variable, ζ. In these equations, prime terms are used to denote arc-length derivatives and dotted terms denote time derivatives.

$$\dot{\zeta} = (V/D)\zeta' \tag{28}$$

$$\ddot{\zeta} = (V/D)^2 (\zeta'' + \zeta' V'/V) \tag{29}$$

Applying the previous assumptions and transformations to the no-roll frame six degree of freedom equations yields equations (30-41).

$$x' = c_\theta D \tag{30}$$

$$y' = c_\theta D\psi + \frac{D}{V}\tilde{v} \tag{31}$$

$$z' = -Ds_\theta + \frac{Dc_\theta}{V}\tilde{w} \tag{32}$$

$$\phi' = \frac{D}{V}\tilde{p} \tag{33}$$

$$\theta' = \frac{D}{V}\tilde{q} \tag{34}$$

$$\psi' = \frac{D}{Vc_\theta}\tilde{r} \tag{35}$$

$$V' = -\frac{\pi\rho D^3}{8m}C_{X0}V - \frac{Dg}{V}s_\theta \tag{36}$$

$$\tilde{v}' = -\frac{\pi\rho D^3}{8m}C_{NA}(\tilde{v} - \tilde{v}_W) - D\tilde{r} \tag{37}$$

$$\tilde{w}' = -\frac{\pi\rho D^3}{8m}C_{NA}(\tilde{w} - \tilde{w}_W) + D\tilde{q} + \frac{Dgc_\theta}{V} \tag{38}$$

$$\tilde{p}' = \frac{\pi\rho V D^4}{8I_{XX}} C_{DD} + \frac{\pi\rho D^5}{16I_{XX}} C_{LP}\tilde{p} \tag{39}$$

$$\tilde{q}' = \frac{\pi\rho D^4 R_{MCM}}{16I_{YY}V} C_{YPA}\tilde{p}(\tilde{v} - \tilde{v}_W) + \frac{\pi\rho D^3 R_{MCP}}{8I_{YY}} C_{NA}(\tilde{w} - \tilde{w}_W) + \frac{\pi\rho D^5}{16I_{YY}} C_{MQ}\tilde{q} - \frac{I_{XX} D}{I_{YY} V}\tilde{p}\tilde{r}_q \tag{40}$$

$$\tilde{r}' = -\frac{\pi\rho D^3 R_{MCP}}{8I_{YY}} C_{NA}(\tilde{v} - \tilde{v}_W) + \frac{\pi\rho D^4 R_{MCM}}{16I_{YY}V} C_{YPA}\tilde{p}(\tilde{w} - \tilde{w}_W) + \frac{I_{XX} D}{I_{YY} V}\tilde{p}\tilde{q} + \frac{\pi\rho D^5}{16I_{YY}} C_{MQ}\tilde{r} \tag{41}$$

Equations (30-41) form the modified linear theory equations of motion for a projectile. These equations, although not strictly linear, are in a form that makes an approximate analytical closed form solution possible.

ANALYTICAL CLOSED FORM SOLUTION

The closed form solutions of equations (30-41) are aided by assuming:

(1) The aerodynamic coefficients are constant.

(2) The total velocity (V) is slowly changing with relation to the other variables. It is only treated as a dynamic variable in the solution of the total velocity equation (36).

(3) The roll rate ($\tilde{p}$) is slowly changing in relation to the other angular rates. It is treated as a dynamic variable in the solution of the roll rate equation, but as a constant in the solution of the epicyclic equations.

With these assumptions, the equations of motion decouple into 5 groups of equations that are largely uncoupled, namely, the total velocity, roll rate, epicyclic, Euler angle, and

swerve equations. The solution process assumes that the epicyclic variables change most rapidly, followed by the total velocity and roll rate. Euler pitch and yaw angle and projectile swerve are assumed to change relatively slowly.

Total Velocity Solution

The total velocity solution expressed in equation (42) is found by treating the pitch angle as a constant and then integrating equation (36).

$$V(s) = \sqrt{\left(V_0^2 + \frac{b_V}{a_V}\right)e^{-2a_V s} - \frac{b_V}{a_V}} \tag{42}$$

The coefficients appearing in equation (42) are:

$$a_V = \frac{\pi\rho D^3}{8m} C_{X0} \qquad b_V = gD\sin(\theta_0) \tag{43}$$

Roll Rate Solution

The roll rate solution is expressed in equation (44).

$$\tilde{p}(s) = C_{pe1}\, e^{C_{pe2}s} - C_{p0} \tag{44}$$

Where:

$$C_{p0} = \frac{2C_{DD}V_0}{DC_{LP}} \qquad C_{pe1} = \tilde{p}_0 + \frac{2C_{DD}V_0}{DC_{LP}} \qquad C_{pe2} = \frac{\pi\rho D^5}{16I_{XX}} C_{LP} \tag{45}$$

Epicyclic Solution

The remaining velocity and angular rate equations (37-38) and (40-41) form a set of coupled non-homogeneous differential equations referred to as the epicyclic equations.

If the pitch angle, total velocity, and roll rate are treated as constant, these equations are linear and can be compacted into the form expressed in equation (46).

$$\begin{Bmatrix} \tilde{v}' \\ \tilde{w}' \\ \tilde{q}' \\ \tilde{r}' \end{Bmatrix} = \begin{bmatrix} -A & 0 & 0 & -D \\ 0 & -A & D & 0 \\ B/D & C/D & E & -F \\ -C/D & B/D & F & E \end{bmatrix} \begin{Bmatrix} \tilde{v} \\ \tilde{w} \\ \tilde{q} \\ \tilde{r} \end{Bmatrix} + \begin{Bmatrix} F_v \\ F_w \\ F_q \\ F_r \end{Bmatrix} \tag{46}$$

The coefficients appearing in equation (46) are expressed in equations (47-55).

$$A = \frac{\pi \rho D^3}{8m} C_{NA} \tag{47}$$

$$B = \frac{\pi \rho D^5 R_{MCM}}{16 I_{YY} V_0} C_{YPA} \tilde{p} \tag{48}$$

$$C = \frac{\pi \rho D^4 R_{MCP}}{8 I_{YY}} C_{NA} \tag{49}$$

$$E = \frac{\pi \rho D^5}{16 I_{YY}} C_{MQ} \tag{50}$$

$$F = \frac{I_{XX} D}{I_{YY} V_0} \tilde{p} \tag{51}$$

$$F_v = A \tilde{v}_{wind} \tag{52}$$

$$F_w = A \tilde{w}_{wind} + \frac{Dgc_{\theta_0}}{V_0} \tag{53}$$

$$F_q = -\frac{B}{D} \tilde{v}_{wind} - \frac{C}{D} \tilde{w}_{wind} \tag{54}$$

$$F_r = -\frac{B}{D} \tilde{w}_{wind} + \frac{C}{D} \tilde{v}_{wind} \tag{55}$$

The Eigen values for this system split into 2 complex pairs, commonly called the fast and slow modes. Equations (56-59) express the closed form solutions for the side velocities, pitch rate, and yaw rate.

$$\begin{aligned}\tilde{v}(s) = C_{v0} &+ e^{\sigma_F s}(C_{vfc}\cos(\Phi_F s) + C_{vfs}\sin(\Phi_F s)) \\ &+ e^{\sigma_S s}(C_{vsc}\cos(\Phi_S s) + C_{vss}\sin(\Phi_S s))\end{aligned} \tag{56}$$

$$\begin{aligned}\tilde{w}(s) = C_{w0} &+ e^{\sigma_F s}(C_{wfc}\cos(\Phi_F s) + C_{wfs}\sin(\Phi_F s)) \\ &+ e^{\sigma_S s}(C_{wsc}\cos(\Phi_S s) + C_{wss}\sin(\Phi_S s))\end{aligned} \tag{57}$$

$$\begin{aligned}\tilde{q}(s) = C_{q0} &+ e^{\sigma_F s}(C_{qfc}\cos(\Phi_F s) + C_{qfs}\sin(\Phi_F s)) \\ &+ e^{\sigma_S s}(C_{qsc}\cos(\Phi_S s) + C_{qss}\sin(\Phi_S s))\end{aligned} \tag{58}$$

$$\begin{aligned}\tilde{r}(s) = C_{r0} &+ e^{\sigma_F s}(C_{rfc}\cos(\Phi_F s) + C_{rfs}\sin(\Phi_F s)) \\ &+ e^{\sigma_S s}(C_{rsc}\cos(\Phi_S s) + C_{rss}\sin(\Phi_S s))\end{aligned} \tag{59}$$

Euler Angle and Swerve Solution

The remaining states are computed through integration of the solutions expressed in equations (42,44,56-59). The variables appear in a linear fashion, after applying the previously discussed assumptions, with the exception of pitch angle (θ) which is operated on by trigonometric functions and appears in terms with other independent variables. In terms in which a trigonometric function of the pitch angle appears as the only independent variable, the integral is approximated by the trapezoid method. When pitch angle appears in a term containing another independent variable, pitch angle is treated as a constant.

$$\phi(s) = C_{\phi 0} + C_{\phi 1}s + C_{\phi e1}e^{C_{\phi e2}s} \tag{60}$$

$$\theta(s) = C_{\theta 0} + C_{\theta 1}s + e^{\sigma_F s}(C_{\theta fc}\cos(\Phi_F s) + C_{\theta fs}\sin(\Phi_F s)) + e^{\sigma_S s}(C_{\theta sc}\cos(\Phi_S s) + C_{\theta ss}\sin(\Phi_S s)) \quad (61)$$

$$\psi(s) = C_{\psi 0} + C_{\psi 1}s + e^{\sigma_F s}(C_{\psi fc}\cos(\Phi_F s) + C_{\psi fs}\sin(\Phi_F s)) + e^{\sigma_S s}(C_{\psi sc}\cos(\Phi_S s) + C_{\psi ss}\sin(\Phi_S s)) \quad (62)$$

$$x(s) = x_0 + \tfrac{1}{2}Ds(\cos(\theta(s)) + \cos(\theta_0)) \quad (63)$$

$$y(s) = C_{y0} + C_{y1}s + C_{y2}s^2 + e^{\sigma_F s}(C_{yfc}\cos(\Phi_F s) + C_{yfs}\sin(\Phi_F s)) + e^{\sigma_S s}(C_{ysc}\cos(\Phi_S s) + C_{yss}\sin(\Phi_S s)) \quad (64)$$

$$z(s) = C_{z0} + C_{z1}s - \tfrac{1}{2}Ds(\sin(\theta(s)) + \sin(\theta_0)) + e^{\sigma_F s}(C_{zfc}\cos(\Phi_F s) + C_{zfs}\sin(\Phi_F s)) + e^{\sigma_S s}(C_{zsc}\cos(\Phi_S s) + C_{zss}\sin(\Phi_S s)) \quad (65)$$

Solution Implementation

Due to the variation of values that are treated as constant in the closed form solution, inaccuracies build in the solution, especially when considering long range indirect fire trajectories. To minimize these inaccuracies, the model is periodically updated along the trajectory. In this process, the last trajectory point computed is treated as the initial conditions for a new trajectory segment. Before the new trajectory segment is computed, all constants in the model are recomputed using the new initial condition data.

The two current methods employed for rapid trajectory prediction are 3 degree of freedom point mass model and conventional linear theory. Both of these methods are limited in their ability to accurately predict a projectile trajectory under general conditions. The three degree of freedom model accounts for high launch angle

trajectories, but ignores rotational dynamics leading to poor swerve prediction. The standard linear theory solution includes rotational dynamics, but is limited to low launch angles. The modified linear theory closed form solution expressed in equations (42,44,56-65) allows rapid and accurate calculation of long range trajectories with large pitch angles.

RESULTS

The capabilities of modified linear theory are shown using simulations of two cases. The first case simulates the short range trajectory of a fin stabilized projectile launched at low pitch angle. The second case simulates a relatively long range trajectory of a spin stabilized projectile launched at high pitch angle. For each case, typical trajectories were computed using four methods; modified linear theory, standard linear theory, 3 degree of freedom numerical simulation, and 6 degree of freedom numerical simulation. The 6 degree of freedom simulation is used as the baseline for validating the other methods. The projectile dynamic model has been previously shown to agree favorably with spark range data [18]. The standard linear theory model is derived and computed similarly to modified linear theory with some differences in the determination of the closed form solutions and the addition of a small pitch angle (θ) assumption [19]. The 3 degree of freedom model, sometimes referred to as the point mass model, treats the projectile as a point mass and applies the zero yaw axial force component directly opposing the aerodynamic velocity. Modified forms of the 3 degree of freedom model have been proposed to account for additional portion of projectile dynamics [19].

Low Launch Angle Trajectory

The projectile used in this simulation is a representative direct fire fin stabilized projectile 25mm in diameter with 6 fins. The projectile weight, mass center measured along the stationline, roll inertia, and pitch inertia are 1.84 N, 0.118 m, 1.15×10^{-5} kg-m^2, and 2.78×10^{-4} kg-m^2 respectively. The projectile initial conditions are as follows: x = 0.0 m, y = 0.0 m, z = 0.0 m, $\phi = 0.0$ deg, $\theta = 2.0$ deg, $\psi = 0.0$ deg, $\tilde{u} = 762$ m/s, $\tilde{v} = 0.0$ m/s, $\tilde{w} = 0.0$ m/s, $\tilde{p} = 10.0$ rad/s, $\tilde{q} = 0.0$ rad/s, and $\tilde{r} = 0.0$ rad/s. The projectile is traveling through the standard atmosphere without wind.

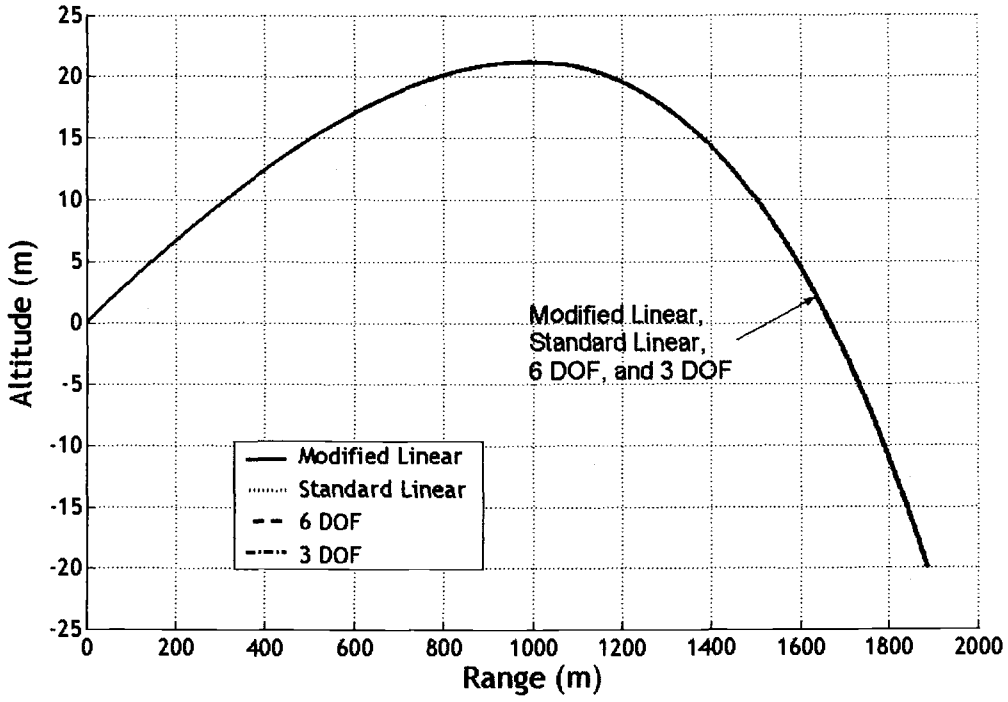

Figure 1.3: Altitude versus range for low launch angle trajectory

Figures 1.3-1.6 compare the trajectories generated by the four prediction methods discussed above. The standard linear theory and modified linear theory trajectories were computed using a dimensionless arc length step size of 100 calibers, which corresponds

to a step of 2.5m for this round and an initial time step of 0.003s at the launch velocity. The 6 degree of freedom and 3 degree of freedom solutions were computed using a time step size of $1.0x10^{-5}$ s.

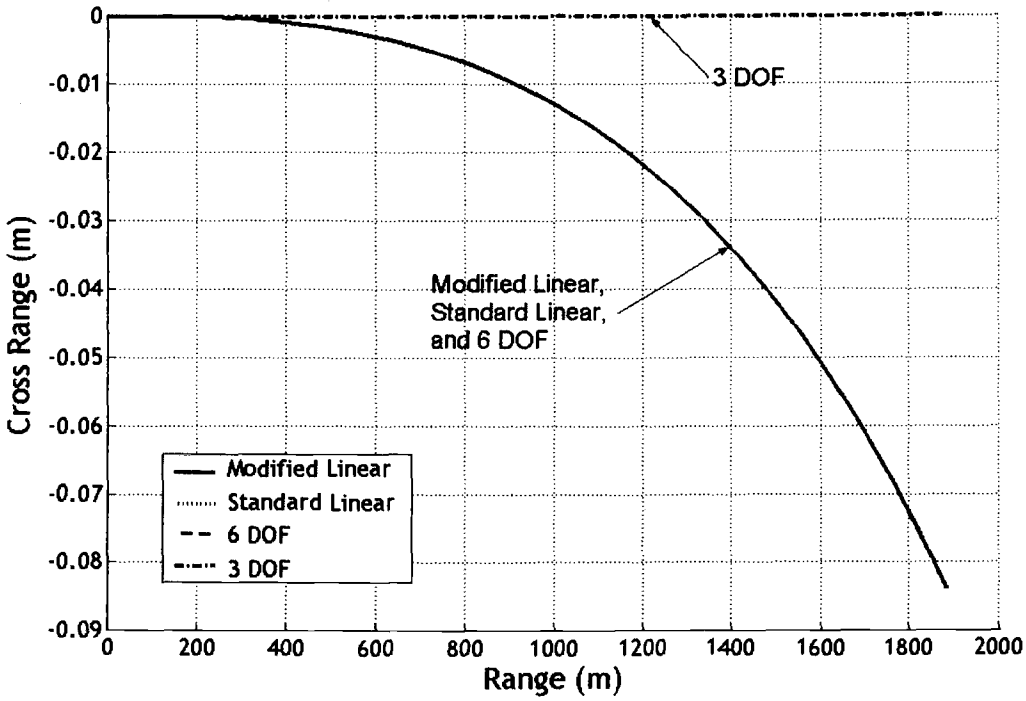

Figure 1.4: Cross range versus range for low launch angle trajectory

Figure 1.3 plots altitude versus downrange distance for each method. Both linear theory models and the 3 degree of freedom model track the trajectory of the projectile predicted by the 6 degree of freedom model quite well. Figure 1.4 plots cross range versus downrange distance for each method. The linear theory models track projectile swerve predicted by the 6 degree of freedom model, while the 3 degree of freedom model predicts no swerve due to the exclusion of rotational dynamics. Figure 1.5 plots velocity versus downrange distance, showing the linear theory models and the 3 degree of freedom model match velocity predicted by the 6 degree of freedom model. Figure 1.6

plots angle of attack versus downrange distance. The modified and the standard linear theory models predict angle of attack well, while the 3 degree of freedom model provides no angle of attack computation.

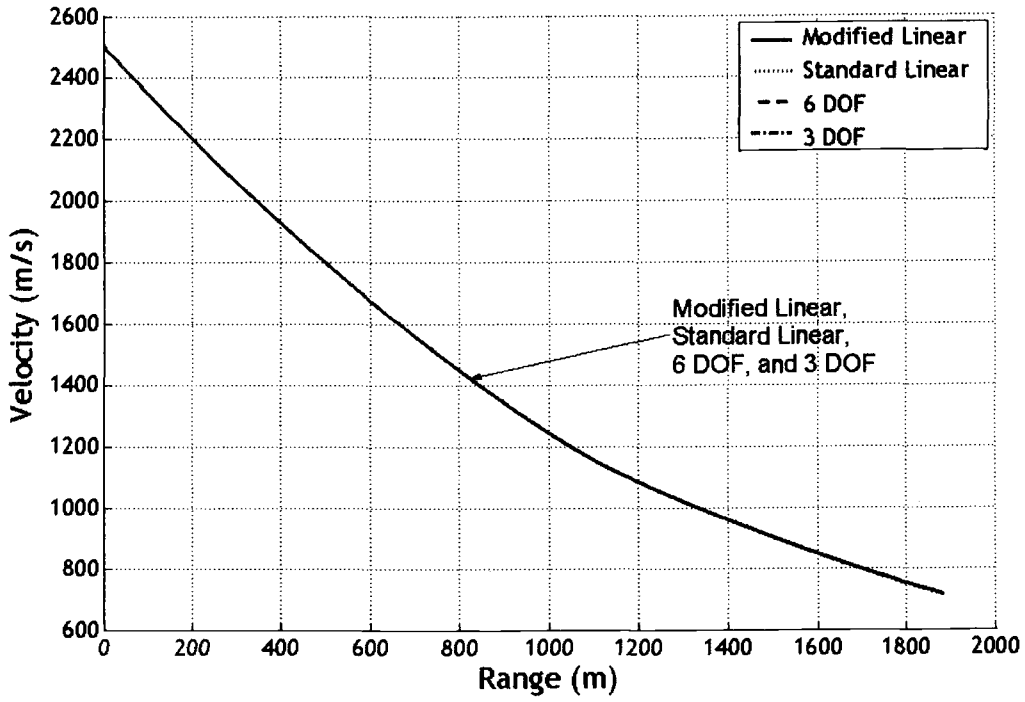

Figure 1.5: Velocity versus range for low launch angle trajectory

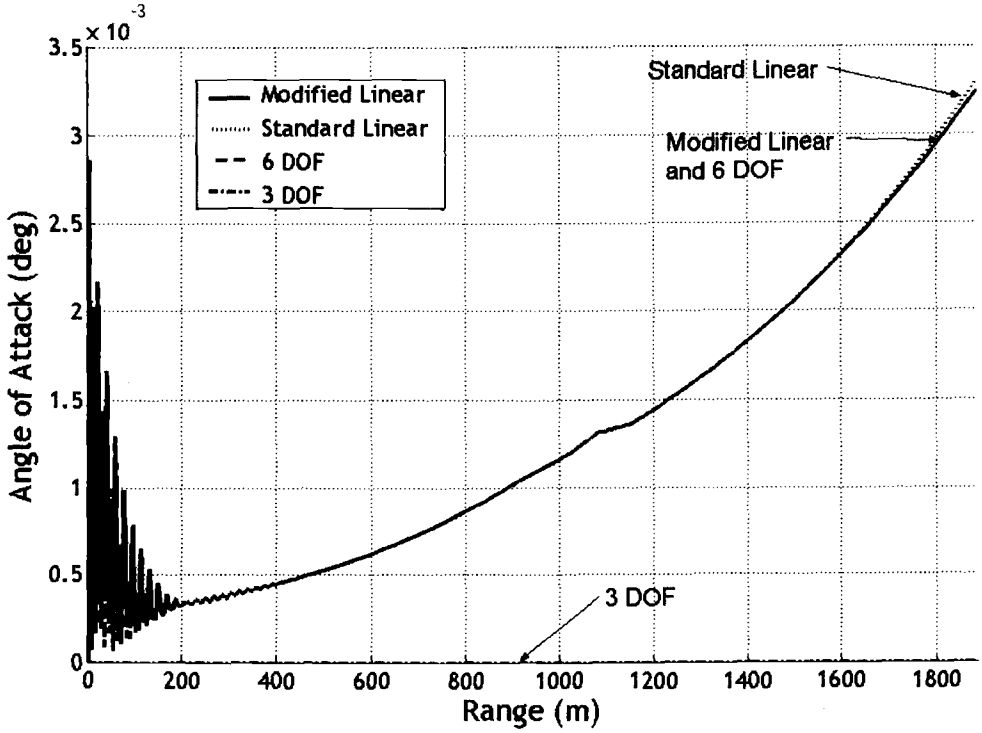

Figure 1.6: Angle of attack versus range for low launch angle trajectory

High Launch Angle Trajectory

The projectile used in this simulation is a representative indirect fire spin stabilized projectile with a diameter of 155mm. The projectile weight, mass center measured along the stationline, roll inertia, and pitch inertia are 422 N, 0.324 m, 0.147 kg-m^2, and 1.893 kg-m^2 respectively. The projectile initial conditions are as follows: x = 0.0 m, y = 0.0 m, z = 0.0 m, ϕ = 0.0 deg, θ = 45.0 deg, ψ = 0.0 deg, $\tilde{u}$ = 853.4 m/s, $\tilde{v}$ = 0.0 m/s, $\tilde{w}$ = 0.0 m/s, $\tilde{p}$ = 1800.0 rad/s, $\tilde{q}$ = 0.0 rad/s, and $\tilde{r}$ = 0.0 rad/s. The projectile is traveling through the standard atmosphere with a 6.1 m/s mean horizontal wind blowing from an angle of 57.3 deg from the down range direction.

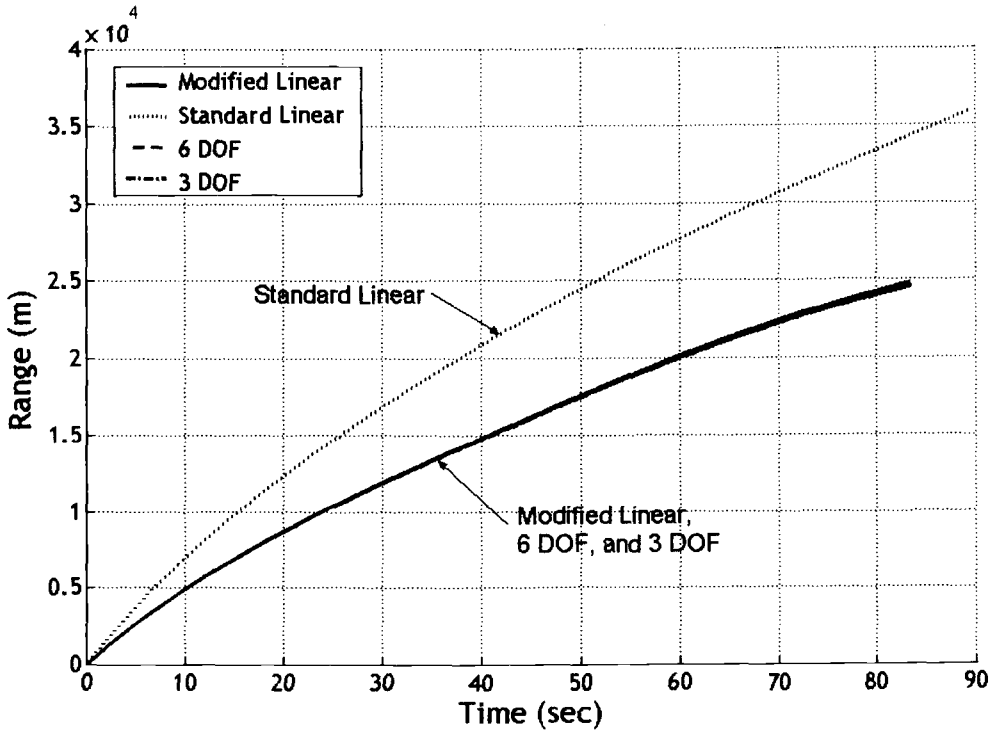

Figure 1.7: Range versus time for high launch angle trajectory

Figures 1.7-1.14 compare trajectories obtained by the four prediction methods discussed above. Standard linear theory and modified linear theory trajectories were computed using a dimensionless arc length step size of 100 calibers, which corresponds to a step of 15.5 m for this round and an initial time step of 0.018s at launch velocity. The 6 degree of freedom and 3 degree of freedom numerical trajectories were computed using a time step size of 1.0×10^{-5} s.

For the high angle shot, modified linear theory is able to predict the trajectory with reasonable accuracy, as shown in figures 1.7-1.14. Figures 1.7, 1.8, and 1.9 show modified linear theory is able to predict the range, altitude, and projectile swerve in wind. Figures 1.10, 1.11, and 1.14 show it accurately accounts for high pitch angles, picks up yaw angle excursions, and predicts angle of attack. Figures 1.12 and 1.13 show that

modified linear theory accurately predicts velocity and roll rate. Standard linear theory, limited by a low launch angle assumption, is unable to accurately predict the simulated trajectory, as seen in figures 1.7-1.14. The three degree of freedom model is able to predict the range, altitude, and velocity reasonably well, as seen in figures 1.7, 1.8, and 1.12, but is unable to generate proper projectile swerve as seen in figure 1.9 and provides no information about the projectile's orientation as seen in figures 1.10 and 1.11, angular rates, or angle of attack as shown in figure 1.14.

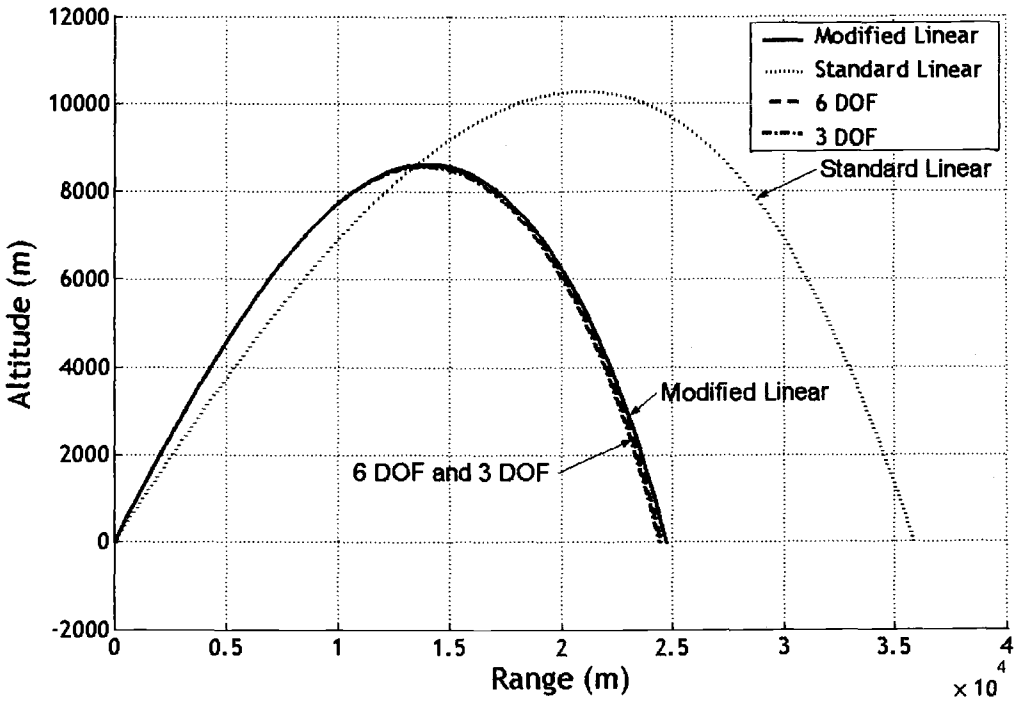

Figure 1.8: Altitude versus range for high launch angle trajectory

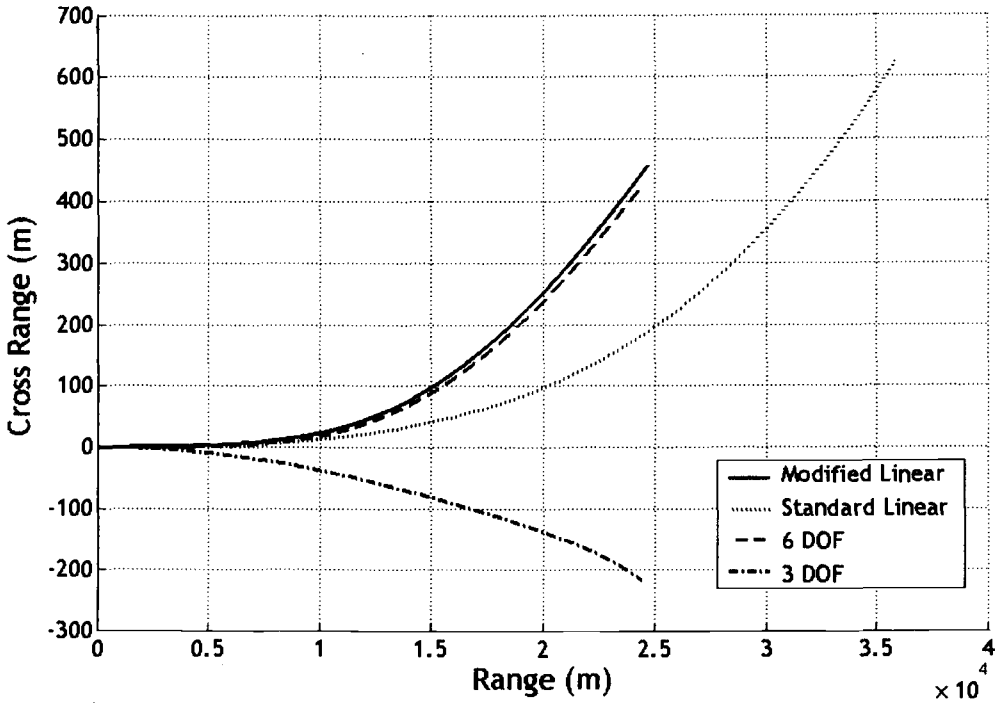

Figure 1.9: Cross range versus range for high launch angle trajectory

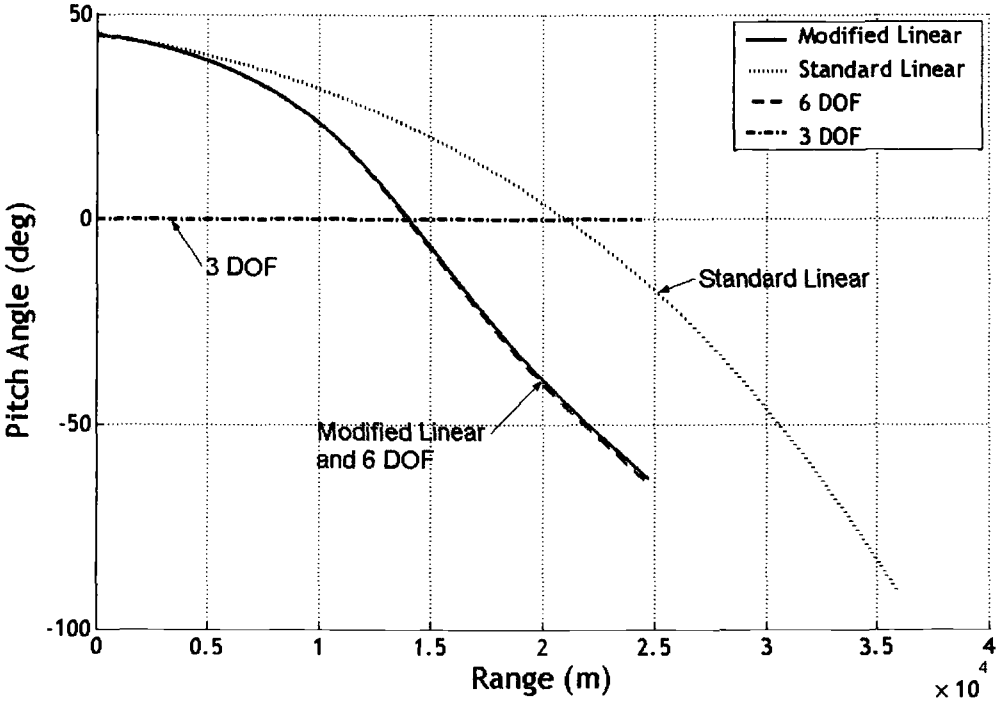

Figure 1.10: Pitch angle versus range for high launch angle trajectory

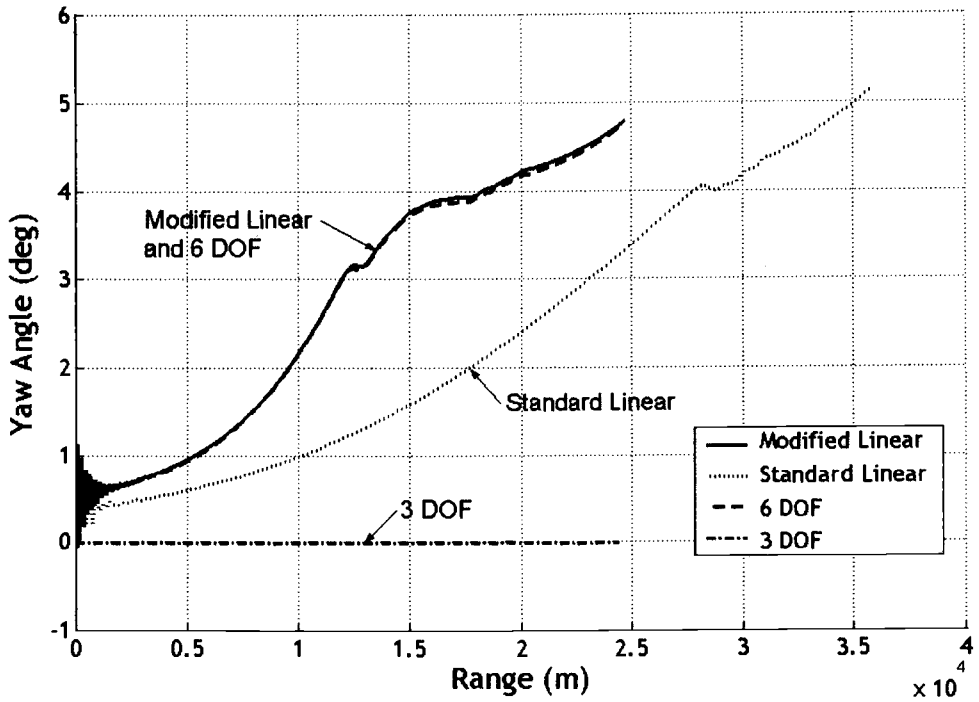

Figure 1.11: Yaw angle versus range for high launch angle trajectory

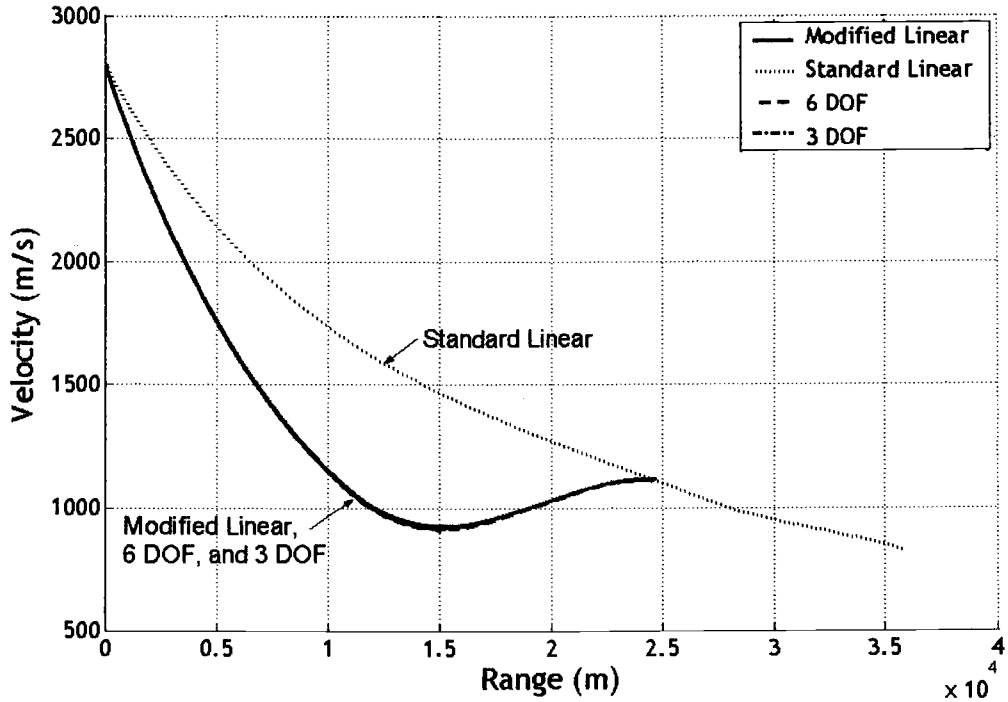

Figure 1.12: Velocity versus range for high launch angle trajectory

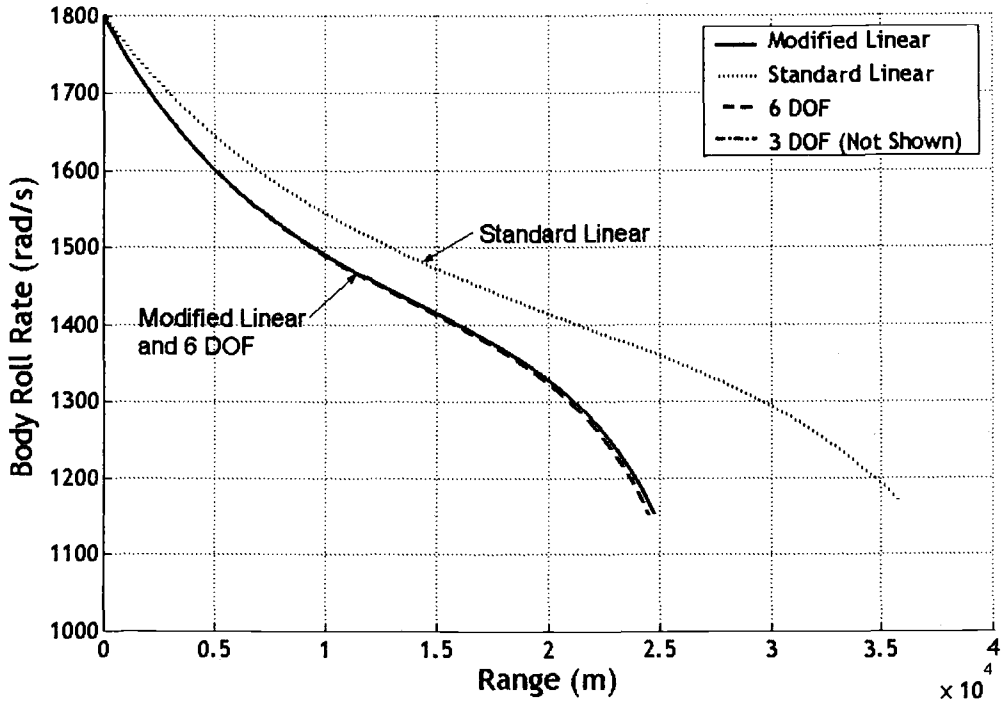

Figure 1.13: Roll rate versus range for high launch angle trajectory

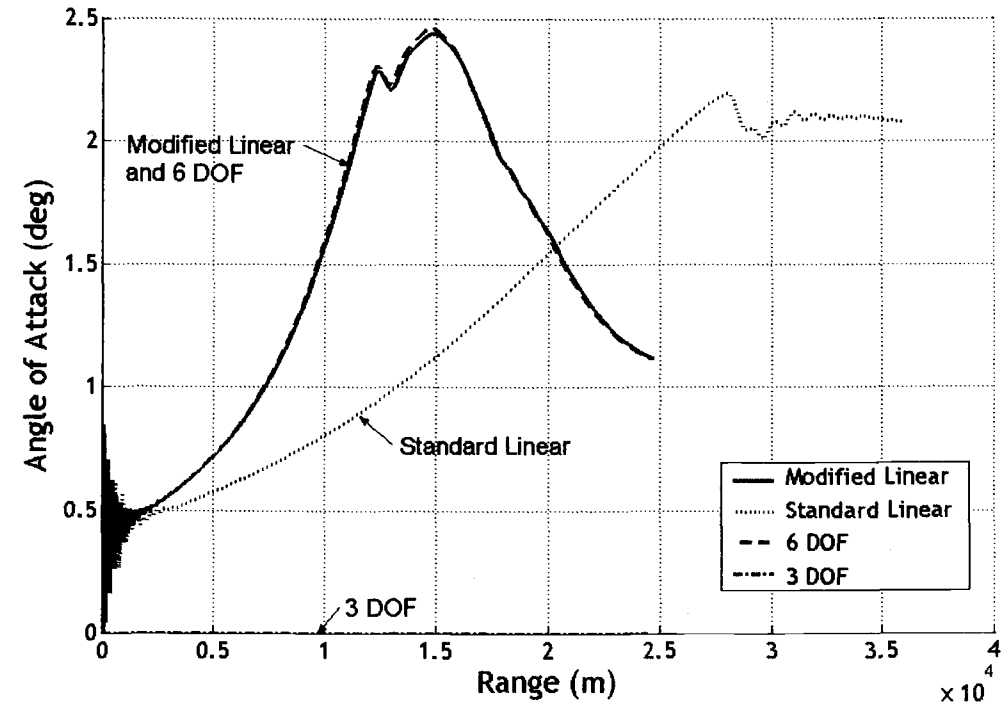

Figure 1.14: Angle of attack versus range for high launch angle trajectory

To highlight modified linear theory's ability to rapidly compute a trajectory the high launch angle trajectory was recomputed using modified linear theory with a step size of 1000 calibers, or 155m. Figures 1.15 and 1.16 compare the yaw angle and the angle of attack predicted by the large step size modified linear theory case to those predicted by the 6 degree of freedom model for the first 3000m of the trajectory. The modified linear theory data in these figures is plotted as the discrete points calculated by each step. These figures show that linear theory can predict the trajectory using a step size that is large enough to skip over the smaller frequencies present in the projectile's motion. By not being limited in step size by the smallest frequency, linear theory is able to rapidly compute future states, such as the impact point, using a relatively small number of steps.

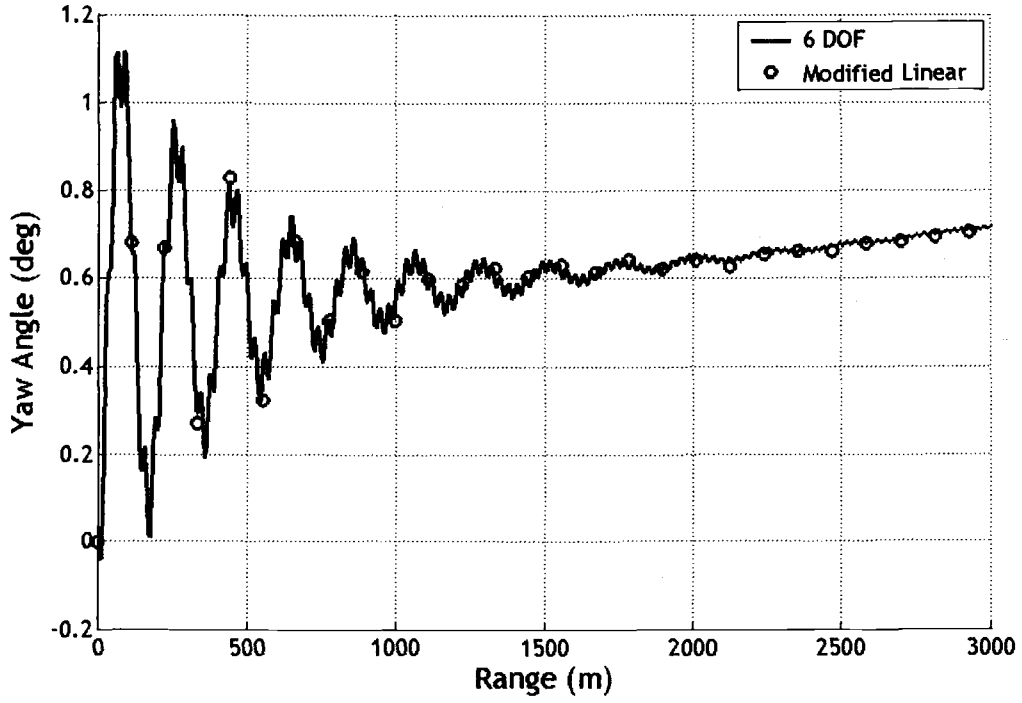

Figure 1.15: Yaw angle versus range for a high launch angle with a large step size

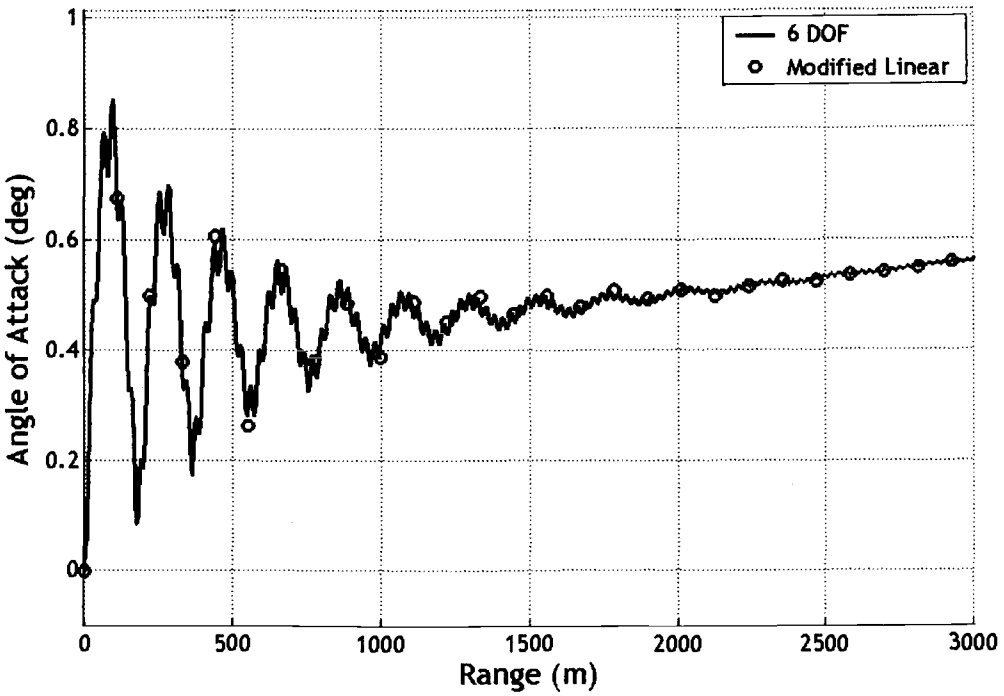

Figure 1.16: Angle of attack versus range for a high launch angle with a large step size

To verify the computational efficiency of modified linear theory, a series of high launch angle trajectories were computed by modified linear theory and a 4^{th} order runge-kutta numerical simulation of the six degree of freedom model at different step sizes and the run times were recorded. A comparison of the times showed that for equivalent step sizes, the modified linear theory model computed the trajectory nearly twice as fast as the 6 degree of freedom model.

CONCLUSIONS

This paper highlights inherent inaccuracies of current methods used to rapidly compute the impact point of a projectile flying a long range trajectory launched at a high gun elevation angle typical of indirect fire smart weapons. Two common methods for rapid trajectory prediction are numerical integration of the point mass dynamic equations

and evaluation of the closed form solution of the rigid body projectile dynamic equations provided by standard linear theory. Numerical integration of the point mass dynamic equations provided satisfactory estimation of range and altitude but generates poor prediction of cross range. Employment of the closed form solution of the projectile rigid body dynamic equations provided by projectile linear theory yields excellent trajectory prediction for short range direct fire shots but estimation accuracy significantly degrades in range, cross range, and altitude for long range shots fired at high gun elevations.

The modified projectile linear theory reported here significantly improves impact point estimation accuracy relative to the other methods mentioned above, particularly for smart indirect fire weapons that are normally fired from a gun with a large elevation angle and also fly long range. While significantly enhancing impact point accuracy, the proposed method is computationally efficient.

REFERENCES

1. Fowler, R., E. Gallop, C. Lock, H. Richmond, "The Aerodynamics of a Spinning Shell," *Philosophical Transactions of the Royal Society of London*, Series A, Vol 221, 1920.
2. Kent, R., "An Elementary Treatment of the Motion of a Spinning Projectile About its Center of Gravity," Ballistic Research Laboratory Report 85, Aberdeen Proving Ground, MD, 1937.
3. Nielson, K., J. Synge, "On the Motion of a Spinning Shell," Ballistic Research Laboratory Report 116, Aberdeen Proving Ground, MD, 1943.

4. Kelley, J., E. McShane, "On the Motion of a Projectile with Small or Slowly Changing Yaw," Ballistic Research Laboratory Report 446, Aberdeen Proving Ground, MD, 1944.

5. Kelley, J., E. McShane, F. Reno, "Exterior Ballistics", University of Denver Press, 1953.

6. Hodapp, A., "Effect of Mass Asymmetry on Ballistic Match of Projectiles," *Journal of Spacecraft and Rockets*, Vol. 13, No. 12, pp. 757-760, 1976.

7. Weber, D., "Simplified Method for Evaluating the Flight Stability of Liquid-Filled Projectiles," *Journal of Spacecraft and Rockets*, Vol. 31, No. 1, pp. 130-134, 1994.

8. Murphy, C., "Angular Motion of a Spinning Projectile with a Viscous Liquid Payload," *Journal of Guidance, Control, and Dynamics,* Vol. 6, No. 4, pp. 280-286, 1983.

9. Cobb, K., R. Whyte, P. Laird, "Effects of a Moving Components on the Motion of a 20-mm Projectile," 11th AIAA Aerodynamics Testing Conference, Mar 18-20, Colorado Springs, CO, USA, pp. 94-103, 1983.

10. Hodapp, A., "Passive Means for Stabilizing Projectiles with Partially Restrained Internal Members", *Journal of Guidance, Control, and Dynamics*, Vol. 12, No. 2, pp. 135-139, 1989.

11. Soper, W., "Projectile Instability Produced by Internal Friction," AIAA Journal, Vol. 16, No. 1, pp. 8-11, 1978.

12. Murphy, C., "Instability of Controlled Projectiles in Ascending or Descending Flight," *Journal of Guidance and Control*, Vol. 4, No. 1, pp. 66-69, 1981.

13. Cooper, G., "Influence of Yaw Cards on the Yaw Growth of Spin Stabilized Projectiles," *Journal of Aircraft*, Vol. 38, No. 2, pp. 266-270, 2001.

14. Guidos, B., G. Cooper, "Closed Form Solution of Finned Projectile Motion Subjected to a Simple In-Flight Lateral Impulse," 38th AIAA Aerospace Sciences Meeting and Exhibit, Reno, NV, Paper No. AIAA-2000-0767, 2000.

15. Costello, M., A. Peterson, "Linear Theory of a Dual-Spin Projectile in Atmospheric Flight, *Journal of Guidance, Control, and Dynamics*, Vol. 23, No. 5, pp. 789-797, 2000.

16. Burchett, B., A. Peterson, M. Costello, "Prediction of Swerving Motion of a Dual-Spin Projectile with Lateral Pulse Jets in Atmospheric Flight," *Mathematical and Computer Modeling*, Vol. 35, No. 1-2, pp. 1-14, 2002.

17. Burchett, B., M. Costello, "Model Predictive Lateral Pulse Jet Control of an Atmospheric Rocket," *Journal of Guidance, Control, and Dynamics*, Vol 25, No 5, pp 860-867, 2002.

18. Costello, M., D. Anderson, "M. Costello, D. Anderson, "Effect of Internal Mass Unbalance on the Terminal Accuracy and Stability of a Projectile," AIAA Paper Number 96-3447, Proceedings of the 1996 AIAA Flight Mechanics Conference, San Diego, CA, 1996.

19. McCoy, R., "Modern Exterior Ballistics", Schiffer Publishing Ltd., Attlen, PA, pp 165-183 & 240-244, 1999.

IN FLIGHT IMPACT POINT PREDICTION

Leonard C. Hainz III and Mark Costello

AIAA Journal of Guidance, Control, and Dynamics

1801 Alexander Bell Drive, Suite 500

Reston, VA 20191-4344

Submitted, In review as of 9/2004

ABSTRACT

A method for real time in-flight prediction of the ground impact point of an indirect fire projectile is investigated. Three sensor configurations are explored, the first assuming that the full projectile state is available at discrete times during flight, the second assuming that inertial position and velocity and angular rates are available at discrete times during the flight, and the third assuming that inertial position and velocity along with roll angle and rate are available at discrete times during flight. The sensor data is blended with an internal projectile model through an extended Kalman filter to obtain an estimate of the projectile state. A six degree of freedom projectile model and a modified linear theory solution are used to propagate the projectile state from an arbitrary point along the trajectory to the ground impact point. Results generated from a previously validated non-linear six degree of freedom projectile model and simulated noisy sensor readings indicate the technique is capable of predicting ground impact to within 15 meters at the apex of the trajectory when full state feedback is available.

NOMENCLATURE

A, B, C, E	epicyclic matrix coefficients
a_V, b_V	velocity solution coefficients
C_*	generic aerodynamic coefficient, defined by subscript
D	projectile reference diameter
ds	discrete arc-length step size

F_v, F_w, F_q, F_r	epicyclic equations forcing coefficients
g	gravity
I	projectile inertia matrix
I_{12}	identity matrix of dimensions 12 by 12
I_{XX}, I_{YY}, I_{ZZ}	diagonal components of the inertia matrix
I_{XY}, I_{YZ}, I_{XZ}	off-diagonal components of the inertia matrix
K_*	generic closed form solution coefficient, defined by subscript
$\tilde{L}, \tilde{M}, \tilde{N}$	external moments on projectile, expressed in the no-roll frame
$\tilde{L}_A, \tilde{M}_A, \tilde{N}_A$	moment due to aerodynamic force, expressed in the no-roll frame
$\tilde{L}_M, \tilde{M}_M, \tilde{N}_M$	moment due to Magnus force, expressed in the no-roll frame
$\tilde{L}_{UA}, \tilde{M}_{UA}, \tilde{N}_{UA}$	unsteady aerodynamic moment, expressed in the no-roll frame
m	mass of projectile
$\tilde{p}, \tilde{q}, \tilde{r}$	projectile roll, pitch, and yaw rates, expressed in the no-roll frame
$R_{\oplus CA}$	vector from the projectile center of mass to the center of pressure
$R_{\oplus CM}$	vector from the projectile center of mass to the Magnus center of pressure
R_{MCM}	distance from center of mass to Magnus center of pressure along station line
R_{MCP}	distance from center of mass to center of pressure along station line
s	dimensionless arc length
t	time
T_{NRI}	transformation matrix from no-roll frame to inertial frame

$\tilde{u},\tilde{v},\tilde{w}$	projectile velocity components, expressed in no-roll frame
$\tilde{u}_A,\tilde{v}_A,\tilde{w}_A$	projectile aerodynamic velocity components, expressed in the no-roll frame
$\tilde{u}_W,\tilde{v}_W,\tilde{w}_W$	wind velocity, expressed in the no-roll frame
V	total velocity
V_A	total aerodynamic velocity
x, y, z	projectile position in inertial space
$\tilde{X},\tilde{Y},\tilde{Z}$	external forces on projectile expressed in the no-roll frame
$\tilde{X}_A,\tilde{Y}_A,\tilde{Z}_A$	aerodynamic force acting on the projectile expressed in the no-roll frame
$\tilde{X}_M,\tilde{Y}_M,\tilde{Z}_M$	Magnus force acting on the projectile expressed in the no-roll frame
$\tilde{X}_w,\tilde{Y}_w,\tilde{Z}_w$	weight force acting on the projectile expressed in the no-roll frame
A	discrete projectile state transition matrix
C	measurement transition matrix
K	Kalman gain matrix
N	model noise correlation matrix
P	state error covariance
P_E	expected state error covariance
Q	model noise covariance matrix
R	measurement noise covariance matrix
X	projectile state vector
X_E	expected projectile state vector
Z	measurement vector

α, β	aerodynamic angles of attack
ϕ	projectile roll angle
θ, ψ	projectile pitch and yaw angles
ρ	atmospheric density
Φ_F, Φ_S	epicyclic Eigen value imaginary components
σ_F, σ_S	epicyclic Eigen value real components

INTRODUCTION

Many powerful smart weapon control techniques rely on accurate observation of the full projectile state. The use of on-board sensors for projectile state observation is plagued by the noise inherent in physical sensors while the use of on-board state propagators is plagued by inaccuracies inherent in simple dynamic models [1]. A widely used observer is the Kalman filter [2-8], which allows for a combination of imperfect information to be blended in a manner that provides an optimal state estimate under specific conditions. Originally formulated by R. Kalman as a state based method for observing discrete linear systems [9], the Kalman filter has been modified and expanded to be effective for a wide range of systems [10].

Aldrich and Krabill developed a missile state estimation scheme for radar tracking data using a Kalman filter algorithm [2]. Improved Kalman filter performance is achieved by altering the bandwidth of the filter based on maneuver of the missile [3]. Speyer and Hull compared several extended Kalman filter

formulations for homing missile guidance. For practical scenarios evaluated they found that standard extended Kalman filter overall performed best relative to the iterated extended Kalman filter, the modified Gaussian second order filter, and the adaptive extended Kalman filter [4]. Chin documented a distributed Kalman filter based navigation system using a strap-down attitude heading reference system blended with G.P.S. [5]. Lam, Pal, Welch, and Grossman developed a magnetometer based attitude determination system with a reduced order Kalman filter. They found that this system is capable of significantly improving spacecraft attitude estimation beyond current non-magnetometer based systems [6]. Burchett and Costello studied the ability of a Kalman filter to estimate projectile sensor bias [7]. Shkolnikov, Shtessel, Zarchan, and Lianos studied performance of the homing interceptor guidance loop using both a sliding mode observer and a Kalman filter. The sliding mode observer produced superior performance for the engagement scenarios reported [8].

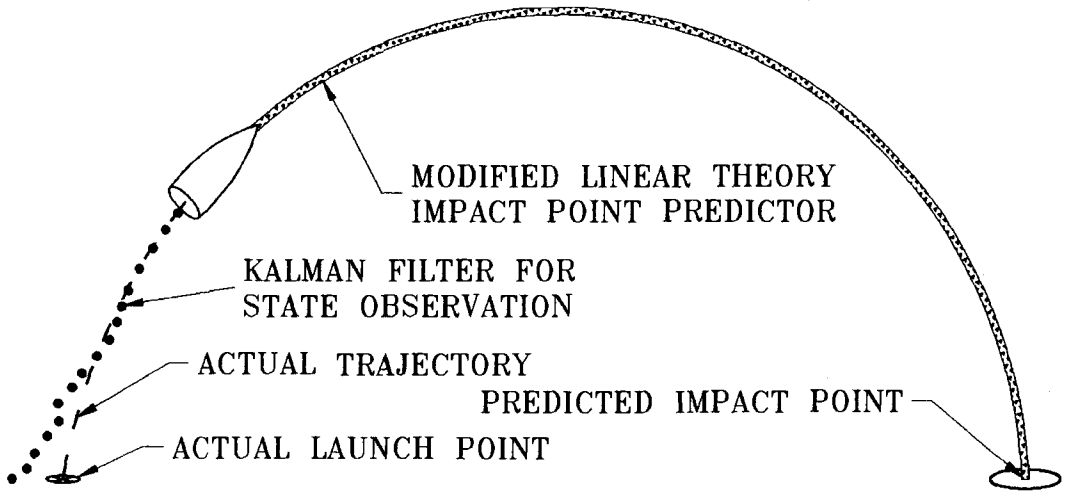

Figure 2.1: Impact Point Estimation Schematic

The work reported here also considers the use of Kalman filtering, but with the application to indirect fire munitions and real time impact point estimation. An extended Kalman filter is used to estimate the projectile state, and the state is propagated to the generating in flight prediction of the impact point of a projectile. A depiction of the overall impact point estimation scheme is shown in Figure 2.1. Three sensor configurations are evaluated. Parametric trade studies considering impact point estimation error under different scenarios are reported.

NONLINEAR PROJECTILE DYNAMIC MODEL

A six degree of freedom rigid projectile model has been proven to accurately simulate the dynamics of a projectile in flight [11]. The six degrees of freedom are comprised of the three translational components describing the position of the

projectile's center of mass, and the three Euler angles describing the orientation of the projectile with respect to a fixed inertial axis. Figures 2.2 and 2.3 provide a schematic of the degrees of freedom. Although commonly expressed and computed in the projectile body frame, the equations of motion for the six degree of freedom model are expressed in the no-roll frame in equations (1-4).

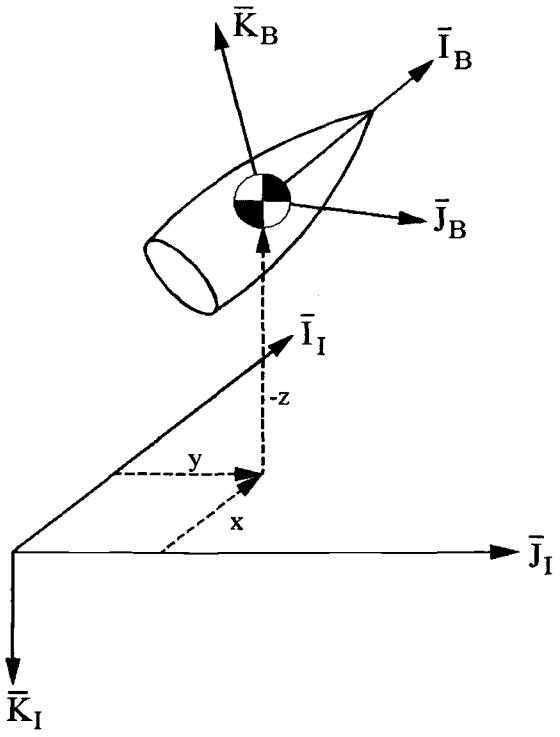

Figure 2.2: Position Definitions

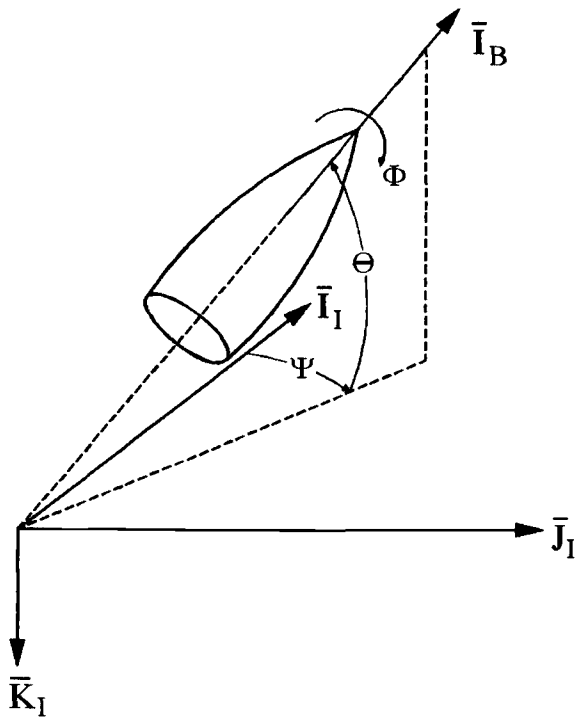

Figure 3: Orientation Definitions

$$\begin{Bmatrix} \dot{x} \\ \dot{y} \\ \dot{z} \end{Bmatrix} = \begin{bmatrix} c_\theta c_\psi & -s_\psi & s_\theta c_\psi \\ c_\theta s_\psi & c_\psi & s_\theta s_\psi \\ -s_\theta & 0 & c_\theta \end{bmatrix} \begin{Bmatrix} \tilde{u} \\ \tilde{v} \\ \tilde{w} \end{Bmatrix} \tag{1}$$

$$\begin{Bmatrix} \dot{\phi} \\ \dot{\theta} \\ \dot{\psi} \end{Bmatrix} = \begin{bmatrix} 1 & 0 & t_\theta \\ 0 & 1 & 0 \\ 0 & 0 & 1/c_\theta \end{bmatrix} \begin{Bmatrix} \tilde{p} \\ \tilde{q} \\ \tilde{r} \end{Bmatrix} \tag{2}$$

$$\begin{Bmatrix} \dot{\tilde{u}} \\ \dot{\tilde{v}} \\ \dot{\tilde{w}} \end{Bmatrix} = \begin{Bmatrix} \tilde{X}/m \\ \tilde{Y}/m \\ \tilde{Z}/m \end{Bmatrix} + \begin{Bmatrix} \tilde{r}\tilde{v} - \tilde{q}\tilde{w} \\ -t_\theta \tilde{r}\tilde{w} - \tilde{r}\tilde{u} \\ \tilde{q}\tilde{u} + t_\theta \tilde{r}\tilde{v} \end{Bmatrix} \tag{3}$$

$$\begin{Bmatrix} \dot{\tilde{p}} \\ \dot{\tilde{q}} \\ \dot{\tilde{r}} \end{Bmatrix} = [I]^{-1} \left(\begin{Bmatrix} \tilde{L} \\ \tilde{M} \\ \tilde{N} \end{Bmatrix} + \begin{bmatrix} 0 & -\tilde{r} & \tilde{q} \\ \tilde{r} & 0 & \tilde{r}t_\theta \\ -\tilde{q} & -\tilde{r}t_\theta & 0 \end{bmatrix} [I] \begin{Bmatrix} \tilde{p} \\ \tilde{q} \\ \tilde{r} \end{Bmatrix} \right) \tag{4}$$

The force acting on the projectile in equation (3) is comprised of the weight force (W) and the aerodynamic force. The aerodynamic force is split into a standard (A) and Magnus (M) aerodynamic force. The combination of forces is expressed in equation (5).

$$\begin{Bmatrix} \tilde{X} \\ \tilde{Y} \\ \tilde{Z} \end{Bmatrix} = \begin{Bmatrix} \tilde{X}_w \\ \tilde{Y}_w \\ \tilde{Z}_w \end{Bmatrix} + \begin{Bmatrix} \tilde{X}_A \\ \tilde{Y}_A \\ \tilde{Z}_A \end{Bmatrix} + \begin{Bmatrix} \tilde{X}_M \\ \tilde{Y}_M \\ \tilde{Z}_M \end{Bmatrix} \tag{5}$$

Equation (6) provides the expression for the weight force in the no-roll coordinate system.

$$\begin{Bmatrix} \tilde{X}_w \\ \tilde{Y}_w \\ \tilde{Z}_w \end{Bmatrix} = mg \begin{Bmatrix} -s_\theta \\ 0 \\ c_\theta \end{Bmatrix} \tag{6}$$

Equation (7) provides the expression for the aerodynamic force in the no-roll coordinate system. This force acts upon the projectile at the aerodynamic center of pressure.

$$\begin{Bmatrix} \tilde{X}_A \\ \tilde{Y}_A \\ \tilde{Z}_A \end{Bmatrix} = -\frac{\pi}{8} \rho V_A^{\,2} D^2 \begin{Bmatrix} C_{X0} + C_{X2}\alpha^2 + C_{X2}\beta^2 \\ C_{Y0} + C_{YB1}\beta \\ C_{Z0} + C_{ZA1}\alpha \end{Bmatrix} \tag{7}$$

Equation (8) provides the expression for the Magnus force in the no-roll coordinate system. The Magnus force acts upon the projectile at the Magnus force center of pressure.

$$\begin{Bmatrix} \tilde{X}_M \\ \tilde{Y}_M \\ \tilde{Z}_M \end{Bmatrix} = \frac{\pi}{8}\rho V_A{}^2 D^2 \begin{Bmatrix} 0 \\ \dfrac{\tilde{p}DC_{NPA}\alpha}{2V_A} \\ \dfrac{-\tilde{p}DC_{NPA}\beta}{2V_A} \end{Bmatrix} \tag{8}$$

Equations (7-8) are based on Mach number dependent coefficients, the aerodynamic angles of attack, and the total aerodynamic velocity.

The moment acting on the projectile in equation (4) is comprised of the moment due to the standard aerodynamic force (A), the moment due to the Magnus aerodynamic force (M), and the unsteady aerodynamic moments (UA) as shown in equation (9).

$$\begin{Bmatrix} \tilde{L} \\ \tilde{M} \\ \tilde{N} \end{Bmatrix} = \begin{Bmatrix} \tilde{L}_A \\ \tilde{M}_A \\ \tilde{N}_A \end{Bmatrix} + \begin{Bmatrix} \tilde{L}_M \\ \tilde{M}_M \\ \tilde{N}_M \end{Bmatrix} + \begin{Bmatrix} \tilde{L}_{UA} \\ \tilde{M}_{UA} \\ \tilde{N}_{UA} \end{Bmatrix} \tag{9}$$

The moment due to the aerodynamic force is expressed in equation (10).

$$\begin{Bmatrix} \tilde{L}_A \\ \tilde{M}_A \\ \tilde{N}_A \end{Bmatrix} = \begin{bmatrix} 0 & -R_{\oplus CAZ} & R_{\oplus CAY} \\ R_{\oplus CAZ} & 0 & -R_{\oplus CAX} \\ -R_{\oplus CAY} & R_{\oplus CAX} & 0 \end{bmatrix} \begin{Bmatrix} \tilde{X}_A \\ \tilde{Y}_A \\ \tilde{Z}_A \end{Bmatrix} \tag{10}$$

The moment due to the Magnus force is expressed in equation (11).

$$\begin{Bmatrix} \tilde{L}_M \\ \tilde{M}_M \\ \tilde{N}_M \end{Bmatrix} = \begin{bmatrix} 0 & -R_{\oplus CMZ} & R_{\oplus CMY} \\ R_{\oplus CMZ} & 0 & -R_{\oplus CMX} \\ -R_{\oplus CMY} & R_{\oplus CMX} & 0 \end{bmatrix} \begin{Bmatrix} \tilde{X}_M \\ \tilde{Y}_M \\ \tilde{Z}_M \end{Bmatrix} \tag{11}$$

The unsteady aerodynamic moments acting on the projectile are expressed in equation (12).

$$\begin{Bmatrix} \tilde{L}_{UA} \\ \tilde{M}_{UA} \\ \tilde{N}_{UA} \end{Bmatrix} = \frac{\pi}{8}\rho V_A{}^2 D^3 \begin{Bmatrix} C_{DD} + \dfrac{\tilde{p}DC_{LP}}{2V_A} \\ \dfrac{\tilde{q}DC_{MQ}}{2V_A} \\ \dfrac{\tilde{r}DC_{NR}}{2V_A} \end{Bmatrix} \tag{12}$$

The coefficients above are projectile specific functions of the Mach number of the projectile.

MODIFIED PROJECTILE LINEAR THEORY

The dynamic equations of motion expressed in equations (1-12) are highly nonlinear. Although the dynamic model expressed above provides a highly accurate method of predicting projectile trajectories, it is computationally cumbersome making it a poor choice for use inside projectile control systems.

Modified projectile linear theory is derived through a series of simplifications to the six degree of freedom equations of motion. These simplifications include negating terms based on relative magnitude, assuming small yaw angles, and converting the independent variable from time, t, to dimensionless arc-length, s. The arc-length, defined in equation (13), is dimensionless and expresses the projectile's downrange travel in calibers.

$$s = \frac{1}{D}\int_0^t V d\tau \tag{13}$$

Equations (14-15) express the relationships between time derivatives and arc-length derivatives in terms of an example variable, ζ. In these equations, prime

terms are used to denote arc-length derivatives and dotted terms denote time derivatives.

$$\dot{\zeta} = (V/D)\zeta' \tag{14}$$

$$\ddot{\zeta} = (V/D)^2 (\zeta'' + \zeta' V'/V) \tag{15}$$

The modified linear theory equations of motion are expressed in equations (16-27).

$$x' = c_\theta D \tag{16}$$

$$y' = c_\theta D\psi + \frac{D}{V}\tilde{v} \tag{17}$$

$$z' = -Ds_\theta + \frac{Dc_\theta}{V}\tilde{w} \tag{18}$$

$$\phi' = \frac{D}{V}\tilde{p} \tag{19}$$

$$\theta' = \frac{D}{V}\tilde{q} \tag{20}$$

$$\psi' = \frac{D}{Vc_\theta}\tilde{r} \tag{21}$$

$$V' = -\frac{\pi\rho D^3}{8m} C_{X0} V - \frac{Dg}{V} s_\theta \tag{22}$$

$$\tilde{v}' = -\frac{\pi\rho D^3}{8m} C_{NA}(\tilde{v} - \tilde{v}_W) - D\tilde{r} \tag{23}$$

$$\tilde{w}' = -\frac{\pi\rho D^3}{8m} C_{NA}(\tilde{w} - \tilde{w}_W) + D\tilde{q} + \frac{Dgc_\theta}{V} \tag{24}$$

$$\tilde{p}' = \frac{\pi\rho V D^4}{8I_{XX}} C_{DD} + \frac{\pi\rho D^5}{16I_{XX}} C_{LP}\tilde{p} \tag{25}$$

$$\tilde{q}' = \frac{\pi\rho D^4 R_{MCM}}{16I_{YY}V} C_{YPA}\tilde{p}(\tilde{v} - \tilde{v}_W) + \frac{\pi\rho D^3 R_{MCP}}{8I_{YY}} C_{NA}(\tilde{w} - \tilde{w}_W) + \frac{\pi\rho D^5}{16I_{YY}} C_{MQ}\tilde{q} - \frac{I_{XX} D}{I_{YY} V}\tilde{p}\tilde{r}_q \tag{26}$$

$$\tilde{r}' = -\frac{\pi\rho D^3 R_{MCP}}{8I_{YY}} C_{NA}(\tilde{v} - \tilde{v}_W) + \frac{\pi\rho D^4 R_{MCM}}{16I_{YY}V} C_{YPA}\tilde{p}(\tilde{w} - \tilde{w}_W) + \frac{I_{XX} D}{I_{YY} V}\tilde{p}\tilde{q} + \frac{\pi\rho D^5}{16I_{YY}} C_{MQ}\tilde{r} \tag{27}$$

Although equations (16-27) are not strictly linear, they are in a form that can be treated as a locally linear set of ordinary differential equations by assuming:

(1) Aerodynamic coefficients are constant.

(2) Total velocity (V) is slowly changing with relation to other variables. It is only treated as a dynamic variable in the solution of the total velocity equation.

(3) Roll rate ($\tilde{p}$) is slowly changing in relation to other angular rates. It is treated as a dynamic variable in the solution of the roll rate equation, but as a constant in the solution of the epicyclic equations.

With these assumptions, the equations of motion decouple into five groups of largely uncoupled equations, namely, the total velocity, roll rate, epicyclic, Euler angle, and swerve equations. The solution process assumes that the epicyclic variables change most rapidly, followed by the total velocity and roll rate. Euler pitch and yaw angle and projectile swerve are assumed to change relatively slowly.

Equations (28-39) express the closed form solutions of the modified linear theory equations of motion. Details on formation of the coefficients in these equations can be found in reference [12].

$$V(s) = \sqrt{\left(V_0^{\,2} + \frac{b_V}{a_V}\right)e^{-2a_V s} - \frac{b_V}{a_V}} \tag{28}$$

$$\tilde{p}(s) = K_{pe1}\,\mathrm{e}^{K_{pe2}s} - K_{p0} \tag{29}$$

$$\begin{aligned}\tilde{v}(s) = K_{v0} &+ e^{\sigma_F s}(K_{vfc}\cos(\Phi_F s) + K_{vfs}\sin(\Phi_F s)) \\ &+ e^{\sigma_S s}(K_{vsc}\cos(\Phi_S s) + K_{vss}\sin(\Phi_S s))\end{aligned} \tag{30}$$

$$\begin{aligned}\tilde{w}(s) = K_{w0} &+ e^{\sigma_F s}(K_{wfc}\cos(\Phi_F s) + K_{wfs}\sin(\Phi_F s)) \\ &+ e^{\sigma_S s}(K_{wsc}\cos(\Phi_S s) + K_{wss}\sin(\Phi_S s))\end{aligned} \tag{31}$$

$$\begin{aligned}\tilde{q}(s) = K_{q0} &+ e^{\sigma_F s}(K_{qfc}\cos(\Phi_F s) + K_{qfs}\sin(\Phi_F s)) \\ &+ e^{\sigma_S s}(K_{qsc}\cos(\Phi_S s) + K_{qss}\sin(\Phi_S s))\end{aligned} \tag{32}$$

$$\begin{aligned}\tilde{r}(s) = K_{r0} &+ e^{\sigma_F s}(K_{rfc}\cos(\Phi_F s) + K_{rfs}\sin(\Phi_F s)) \\ &+ e^{\sigma_S s}(K_{rsc}\cos(\Phi_S s) + K_{rss}\sin(\Phi_S s))\end{aligned} \tag{33}$$

$$\phi(s) = K_{\phi 0} + K_{\phi 1}s + K_{\phi e1}e^{C_{\phi e2}s} \tag{34}$$

$$\begin{aligned}\theta(s) = K_{\theta 0} + K_{\theta 1}s &+ e^{\sigma_F s}(K_{\theta fc}\cos(\Phi_F s) + K_{\theta fs}\sin(\Phi_F s)) \\ &+ e^{\sigma_S s}(K_{\theta sc}\cos(\Phi_S s) + K_{\theta ss}\sin(\Phi_S s))\end{aligned} \tag{35}$$

$$\begin{aligned}\psi(s) = K_{\psi 0} + K_{\psi 1}s &+ e^{\sigma_F s}(K_{\psi fc}\cos(\Phi_F s) + K_{\psi fs}\sin(\Phi_F s)) \\ &+ e^{\sigma_S s}(K_{\psi sc}\cos(\Phi_S s) + K_{\psi ss}\sin(\Phi_S s))\end{aligned} \tag{36}$$

$$x(s) = x_0 + \tfrac{1}{2}Ds(\cos(\theta(s)) + \cos(\theta_0)) \tag{37}$$

$$y(s) = K_{y0} + K_{y1}s + K_{y2}s^2 + e^{\sigma_F s}(K_{yfc}\cos(\Phi_F s) + K_{yfs}\sin(\Phi_F s)) + e^{\sigma_S s}(K_{ysc}\cos(\Phi_S s) + K_{yss}\sin(\Phi_S s)) \quad (38)$$

$$z(s) = K_{z0} + K_{z1}s - \tfrac{1}{2}Ds(\sin(\theta(s)) + \sin(\theta_0)) + e^{\sigma_F s}(K_{zfc}\cos(\Phi_F s) + K_{zfs}\sin(\Phi_F s)) + e^{\sigma_S s}(K_{zsc}\cos(\Phi_S s) + K_{zss}\sin(\Phi_S s)) \quad (39)$$

STATE ESTIMATION

In order to combine measured data with the projectile dynamic model, a Kalman filter is employed. When the underlying statistical properties are Gaussian, the Kalman filter is known to be an optimal state estimator. Through the combination of measurements and model data, the Kalman filter is able to provide a relatively accurate state estimation when presented with model inaccuracies, measurement errors, initial condition errors, and partial state measurements.

The discrete Kalman filter designed to estimate the projectile state is a recursive algorithm consisting of five steps. The first step is in this process is propogation of the projectile state to the time of the next measurement by stepping the dynamic model forward in time. Equation (40) defines the state vector of the projectile, denoted as $\mathbf{X}$.

$$\mathbf{X} = [x, y, z, \phi, \theta, \psi, V, \tilde{v}, \tilde{w}, p, \tilde{q}, \tilde{r}]^T \quad (40)$$

Equation (41) expresses the modified linear theory closed form solutions used to propagate the state to the expected state value at the time of the next measurement.

$$\mathbf{X}_E(s+ds) = f(\mathbf{X}(s), ds) \tag{41}$$

Equation (42) defines the discrete linearized state propagation equation, which contains the discrete state transition matrix, $\mathbf{A}$.

$$\mathbf{X}(s+ds) = \mathbf{A}\mathbf{X}(s) + \mathbf{B} \tag{42}$$

The second step in the Kalman filter algorithm is propagating the state error covariance to the time of the next measurement. Equation (43) provides the expression for the expected covariance at the time of the next measurement.

$$\mathbf{P}_E(s+ds) = \mathbf{A}\,\mathbf{P}(s)\mathbf{A}^{\mathrm{T}} + \mathbf{N}\,\mathbf{Q}\,\mathbf{N}^{\mathrm{T}} \tag{43}$$

The third step in the estimation process is computation of the Kalman gain. Equation (44) provides the Kalman gain as a combination of the expected state from step one and the expected state error covariance estimated in step two.

$$\mathbf{K} = \mathbf{P}_E(s+ds)\mathbf{C}^T\left(\mathbf{C}\mathbf{P}_E(s+ds)\mathbf{C}^T + \mathbf{R}\right)^{-1} \tag{44}$$

Equation (45) expresses the measurement relationship, in which the measurement matrix, $\mathbf{C}$, defines a linear relationship between the state and the measurement.

$$\mathbf{Z} = \mathbf{C}\mathbf{X} \tag{45}$$

The fourth step in the estimation process utilizes a least squares recursive relationship to update the projectile state estimate. Equation (46) provides the updated projectile state estimation as a combination of the measurement, the expected state value from step one, and the Kalman gain from step three.

$$\mathbf{X}(s+ds) = \mathbf{X}_E(s+ds) + \mathbf{K}\left(\mathbf{Z}(s+ds) - \mathbf{C}\mathbf{X}_E(s+ds)\right) \tag{46}$$

The fifth and final step in the recursive algorithm is an update of the projectile state error covariance. Equation (47) provides the updated projectile state error covariance as a combination of the estimated state error covariance from step two, and the Kalman gain from step three.

$$\mathsf{P}(s+ds) = \left(I_{12} - \mathsf{KC}\right)\mathsf{P}_E(s+ds)\left(I_{12} - \mathsf{KC}\right)^T + \mathsf{K}\,\mathsf{R}\,\mathsf{K}^T \tag{47}$$

IMPACT POINT PREDICTION

Prediction of a projectile's impact point from an arbitrary point in the trajectory is considered using two propagation methods. The projectile state estimate at the given instant is propagated to the impact area using either a numerical simulation of the six degree of freedom model or the modified linear theory state propagation equations (28-39). The six degree of freedom model is included as an optimal impact point predictor, allowing a discussion of filter performance. Due to the approximate nature of modified projectile linear theory, accuracy of trajectory prediction over relatively large horizons is significantly aided by splitting the remaining trajectory into a number of elements. At the beginning of each segment, all Mach number dependent coefficients are recomputed using the total velocity estimate at the beginning of the segment. When an impact occurs within a segment, the actual impact point is predicted through linear interpolation between the non-impacted and the impacted states.

RESULTS

The capabilities of the in flight estimator are exercised by considering three sensor configurations. The first sensor configuration assumes full state feedback while the second and third sensor configurations assume a partial state measurement consisting of nine and eight measurements respectively. For each sensor configuration, state estimations are created from simulated measurements based on a nominal trajectory. State estimation is then propagated using both a six degree of freedom and a modified linear theory impact point estimator.

The projectile used in this simulation is a representative indirect fire spin stabilized projectile with a diameter of 155 mm. The projectile weight, mass center measured along the stationline, roll inertia, and pitch inertia are 422 N, 0.324 m, 0.147 kg·m^2, and 1.893 kg·m^2 respectively. The nominal projectile initial conditions are as follows: x = 0.0 m, y = 0.0 m, z = 0.0 m, ϕ = 0.0 deg, θ = 30.0 deg, ψ = 0.0 deg, $\tilde{u}$ = 609.6 m/s, $\tilde{v}$ = 0.0 m/s, $\tilde{w}$ = 0.0 m/s, $\tilde{p}$ = 2000.0 rad/s, $\tilde{q}$ = 0.0 rad/s, and $\tilde{r}$ = 0.0 rad/s. The ground impact point of the nominal trajectory is at a downrange distance of 14,990 m and a cross range distance of 270 m. The ground impact occurs at 47.0 s after launch, and apex of the trajectory occurs at 21.9 s.

Position, Orientation, Velocity, and Angular Velocity Measurement

The measurement model used in this set of simulations assumes the entire state, with the addition of noise, is available from the sensors at a rate of 100 Hz. The measurements have simulated Gaussian noise superimposed as detailed in Table 1.

Table 1: Measurement Error Magnitudes

Full State Feedback		9 Measurements		8 Measurements	
	Noise Standard Deviation		Noise Standard Deviation		Noise Standard Deviation
x	1.60 m	x	1.60 m	x	1.60 m
y	1.60 m	y	1.60 m	y	1.60 m
z	1.60 m	z	3.60 m	z	3.60 m
ϕ	4.7 deg	$\dot{x}$	0.025 m/s	$\dot{x}$	0.025 m/s
θ	4.7 deg	$\dot{y}$	0.025 m/s	$\dot{y}$	0.025 m/s
ψ	4.7 deg	$\dot{z}$	0.030 m/s	$\dot{z}$	0.040 m/s
$\tilde{u}$	1.52 m/s	$\tilde{p}$	0.001 rad/s	ϕ	1.0 deg
$\tilde{v}$	0.030 m/s	$\tilde{q}$	0.001 rad/s	$\dot{\phi}$	0.0 rad/s
$\tilde{w}$	0.030 m/s	$\tilde{r}$	0.001 rad/s		
$\tilde{p}$	0.10 rad/s				
$\tilde{q}$	0.001 rad/s				
$\tilde{r}$	0.001 rad/s				

Figures 2.4-2.15 compare the trajectories generated by various components of the impact point estimator with the nominal projectile trajectory. For demonstration purposes the filter was initialized with relatively large errors: δx = 152.4 m, δy = 30.5 m, $\delta\theta$ = 5.5 deg, $\delta\tilde{u}$ = 61.0 m/s, $\delta\tilde{v}$ = 1.5 m/s, $\delta\tilde{w}$ = 1.5 m/s, $\delta\tilde{p}$ = -200.0 rad/s, $\delta\tilde{q}$ = 0.01 rad/s, and $\delta\tilde{r}$ = 0.01 rad/s. Figures 2.4-2.15 plot 4

traces. The nominal projectile trajectory, as computed by a six degree of freedom numerical simulation, is represented by a solid line. The state estimate provided by the Kalman filter is represented by a dotted line. The dashed line represents the propagation to impact of the Kalman filter's initial conditions. The dash-dot line represents the propagation to impact of the state estimated by the Kalman filter at the projectile trajectory apex. The apex of the Kalman filtered trajectory is marked with a diamond. Figure 2.4 plots range versus time showing that the initial condition trajectory impacts the ground 10 second after the projectile trajectory while both the Kalman filter trajectory and the propagated apex trajectory predict the projectile impact point. Figure 2.5 plots altitude versus range showing the overshoot of the initial condition trajectory to be approximately 3000 m. Figure 2.6 plots cross range versus range and Figure 2.7 plots pitch angle versus range. In these plots the Kalman filter trajectory begins at the initial conditions and begins tracking the projectile trajectory within 2000 m of flight. Figure 2.8 plots yaw angle versus range showing a spike in yaw angle predicted by the Kalman filter followed by an asymptotic return to tracking projectile yaw angle within 2000 m of launch. Figure 2.11 plots total velocity versus range and Figure 2.12 plots roll rate versus range. Both figures show the Kalman filter trajectory beginning at the initial conditions and rapidly tracking the projectile trajectory. Figure 2.10 plots side velocity versus range, Figure 2.11 plots vertical velocity versus range, Figure 2.13 plots pitch rate versus range, and Figure 2.14 plots yaw rate versus range. In these plots, the Kalman filtered trajectory tracks the projectile trajectory but with the inclusion of

noise. Figure 2.15 plots angle of attack versus range showing the Kalman filtered trajectory tracking the projectile trajectory with the inclusion of noise. Although some noise is seen in the side velocities, pitch rate, and yaw rate the Kalman filter is capable of predicting the trajectory of a projectile when initialized with inaccurate conditions and provided with noisy measurements.

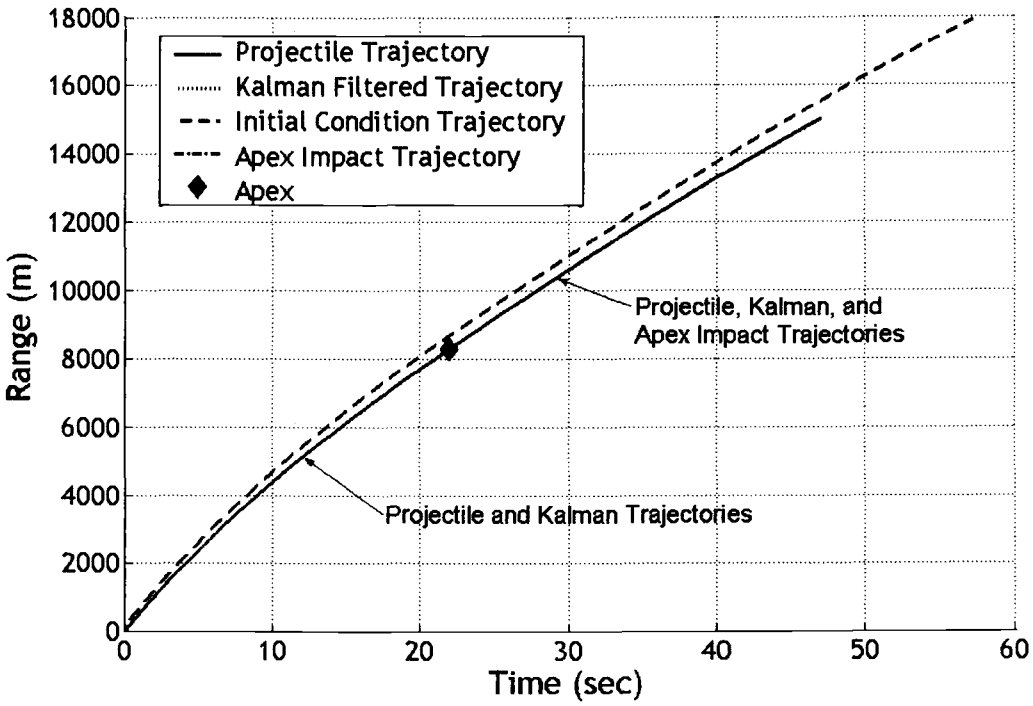

Figure 2.4: Range versus Time

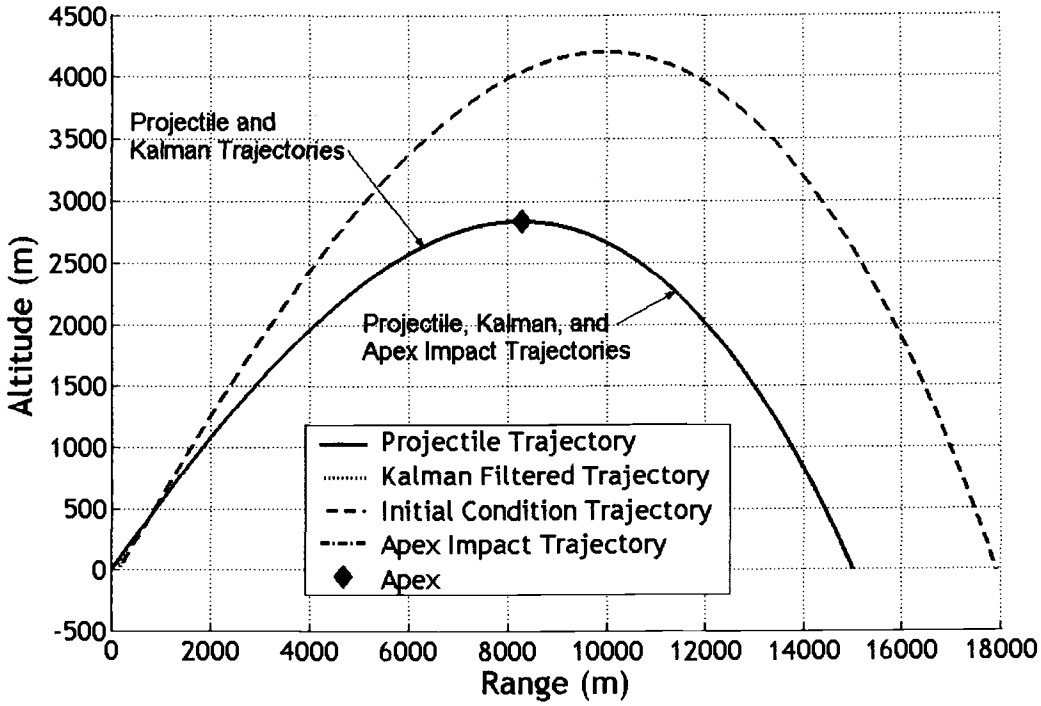

Figure 2.5: Altitude versus Range

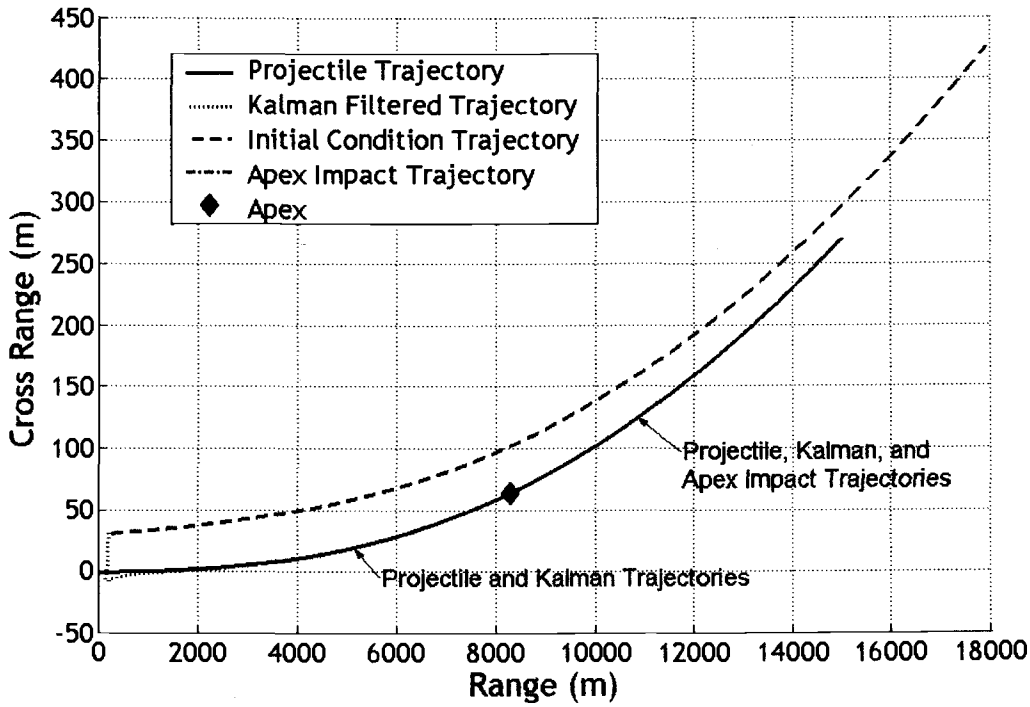

Figure 2.6: Cross Range versus Range

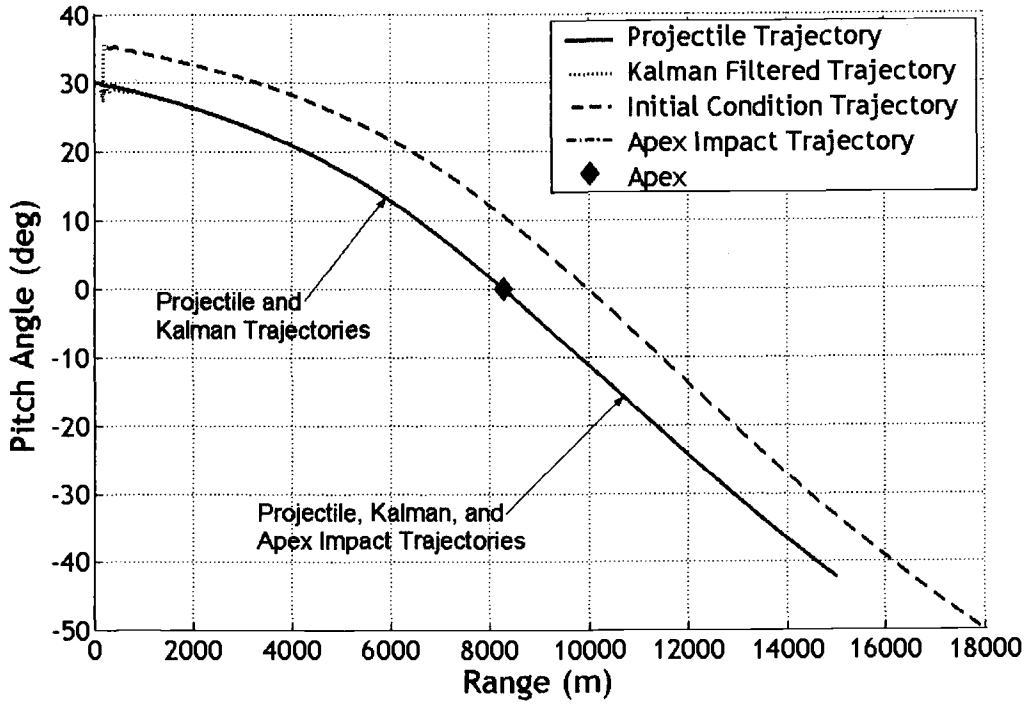

Figure 2.7: Pitch Angle versus Range

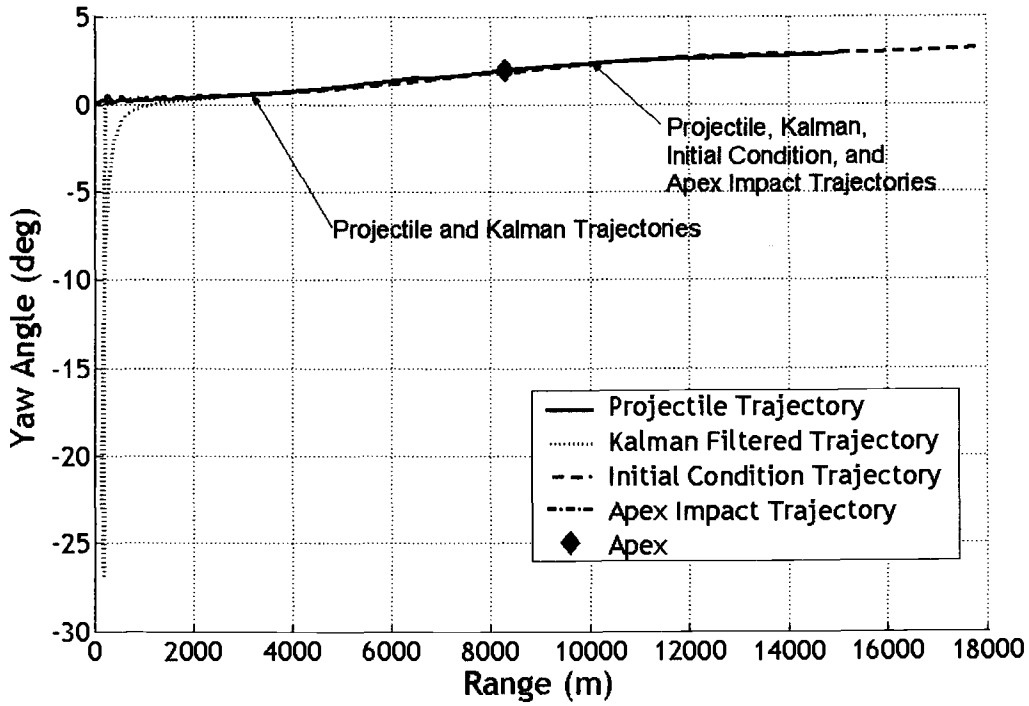

Figure 2.8: Yaw Angle versus Range

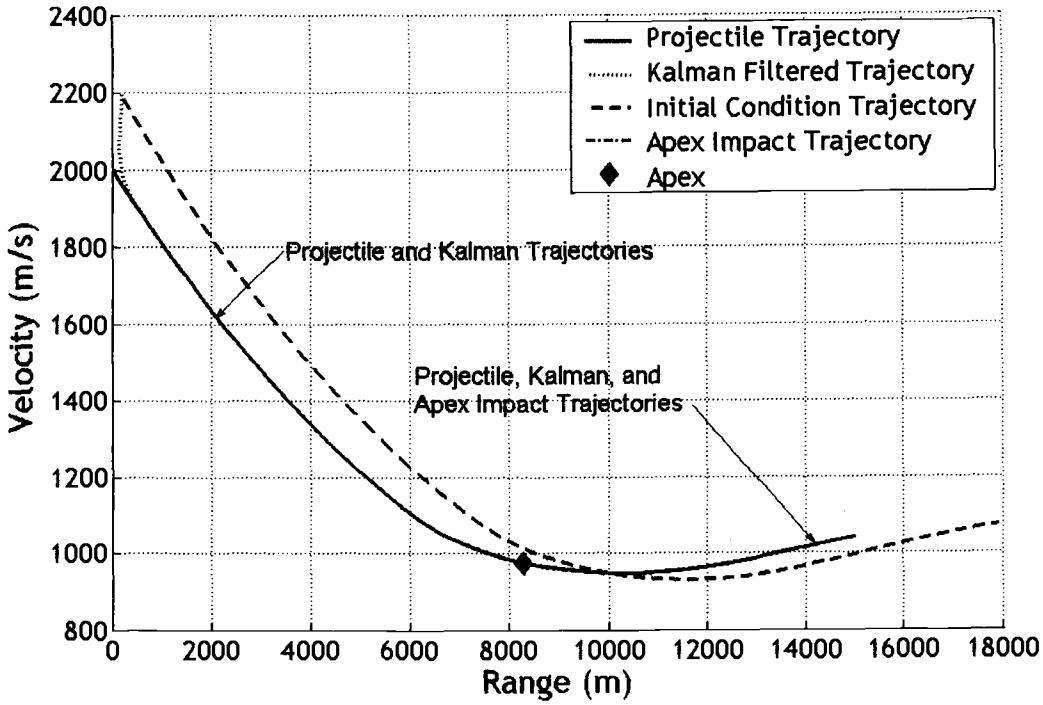

Figure 2.9: Total Velocity versus Range

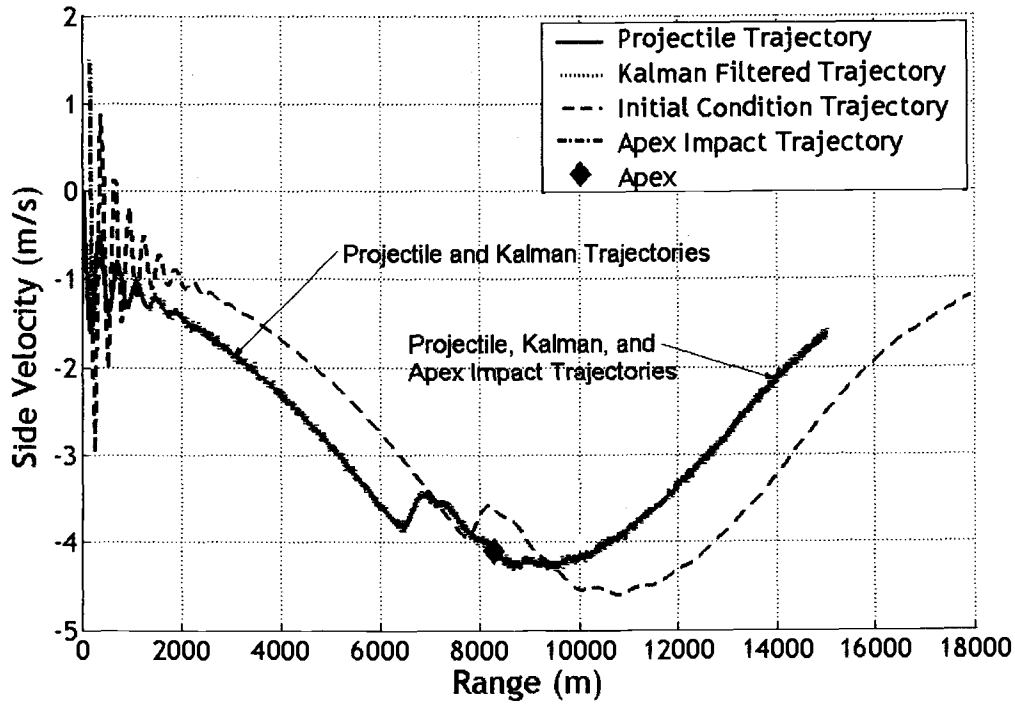

Figure 2.10: Side Velocity versus Range

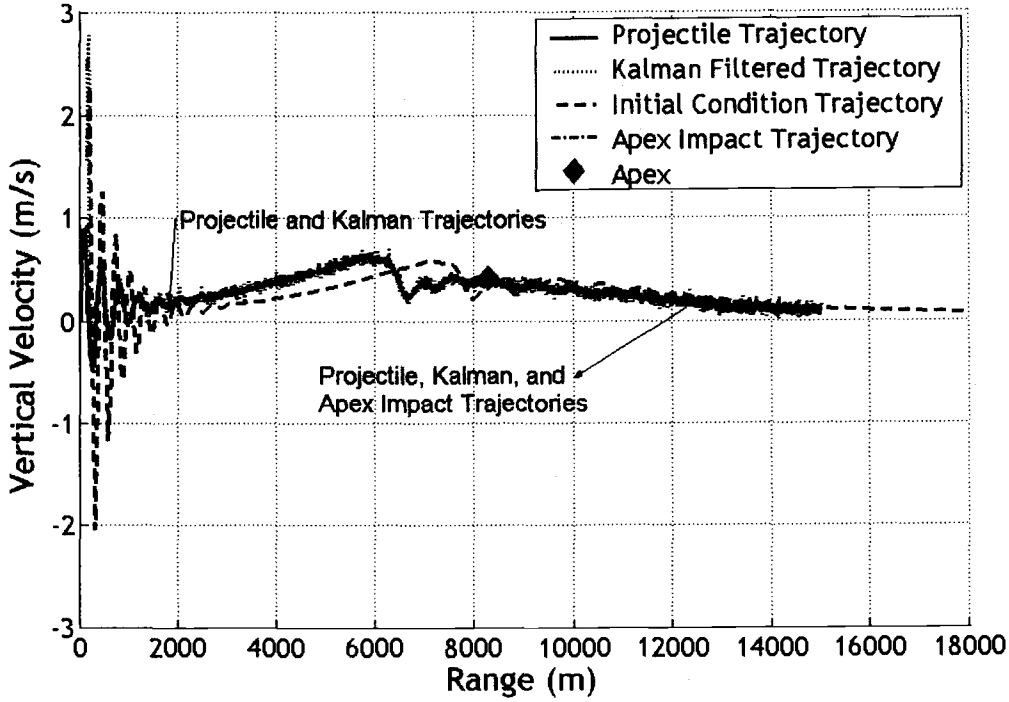

Figure 2.11: Vertical Velocity versus Range

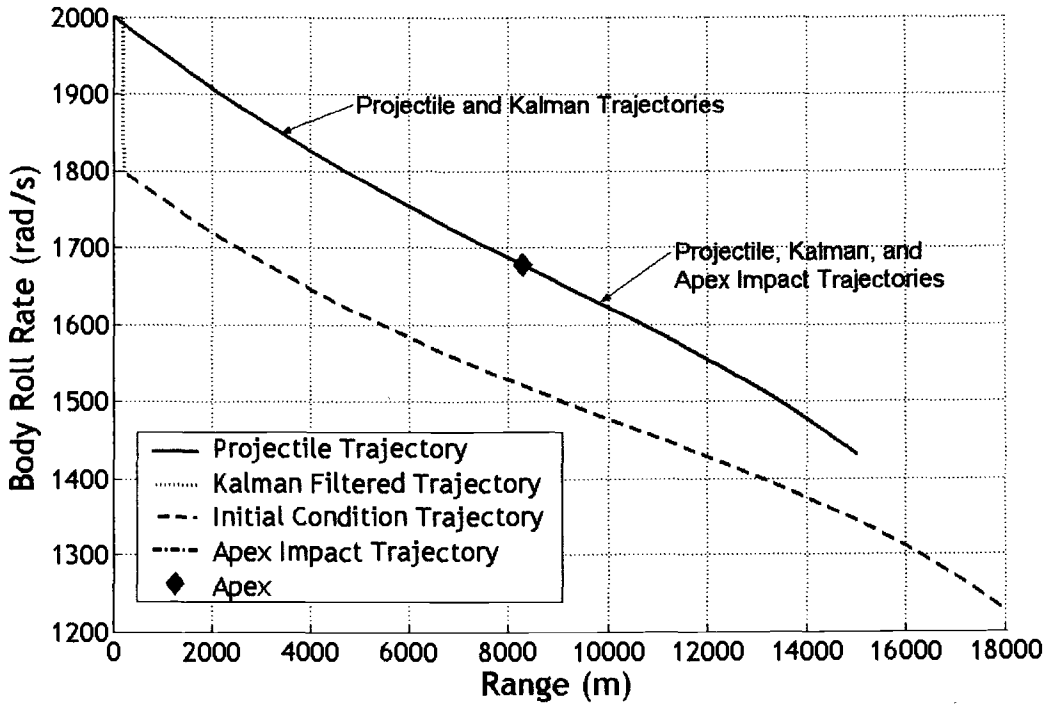

Figure 2.12: Roll Rate versus Range

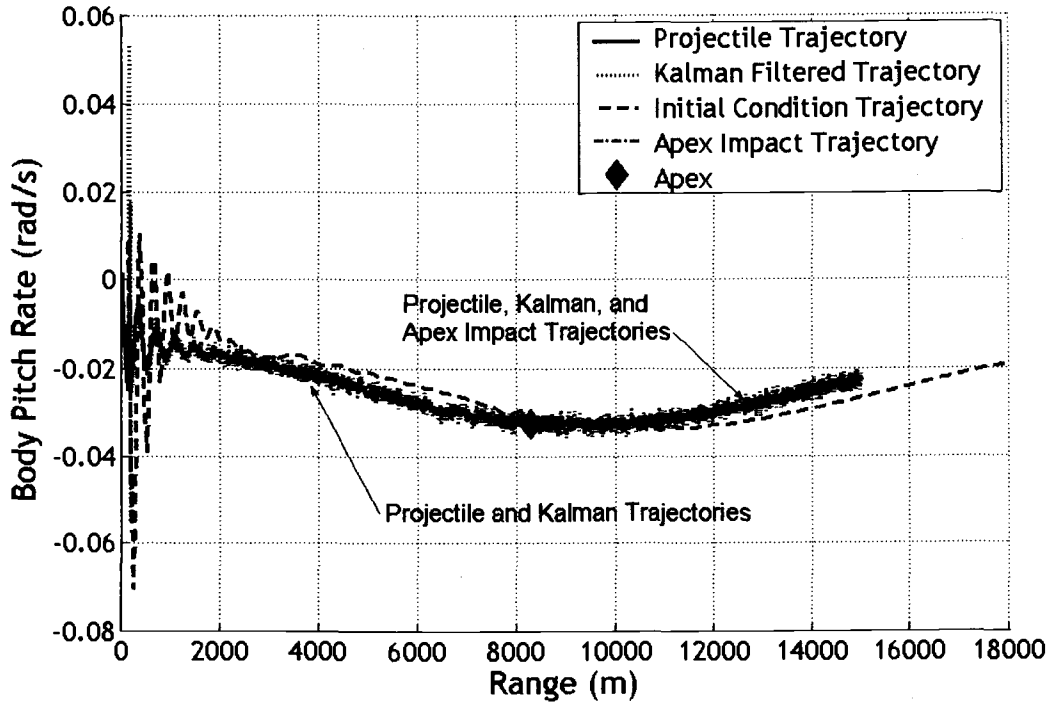

Figure 2.13: Pitch Rate versus Range

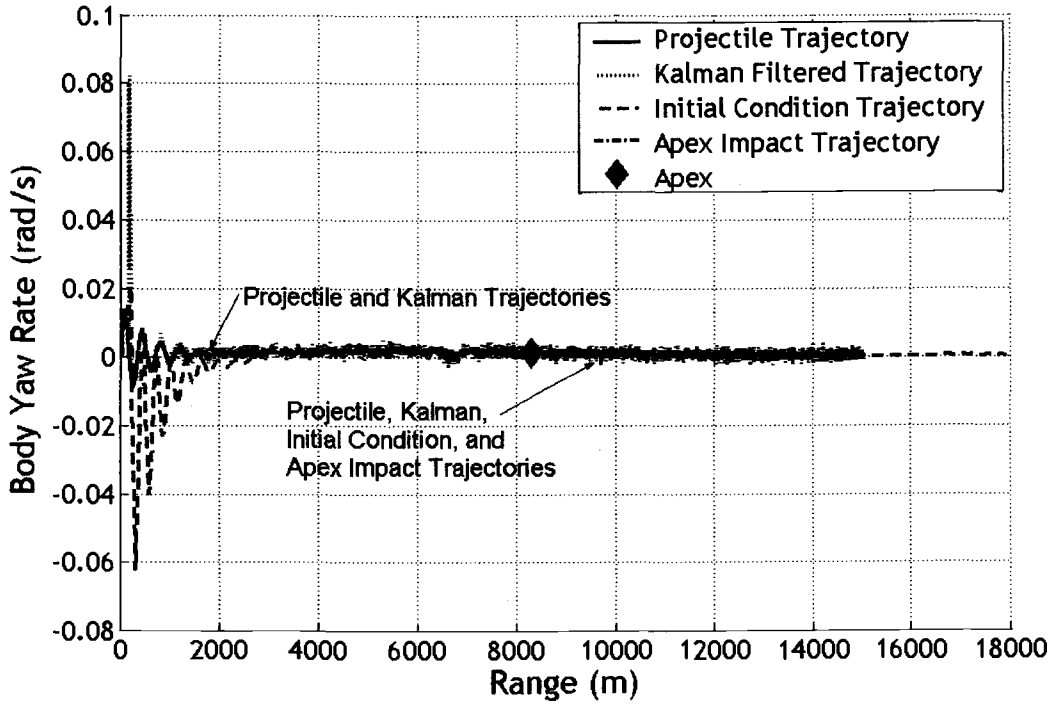

Figure 2.14: Yaw Rate versus Range

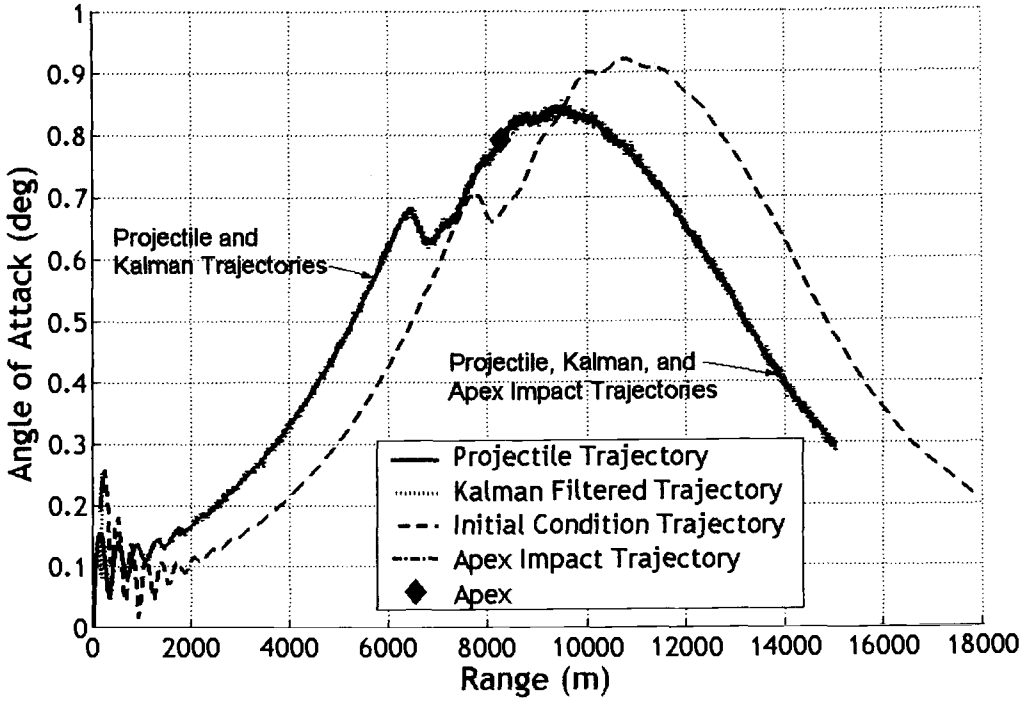

Figure 2.15: Angle of Attack versus Range

Figure 2.16 shows the magnitude of the error in predicted impact point as a function of time for both the six degree of freedom and the modified linear theory impact point estimators. For both impact estimators, the average error for ten simulations with differing simulated measurement noise is shown. At the apex of the trajectory, the predicted impact point has an error of less than 15 m for the six degree of freedom impact point estimator and less than 41 m for the modified linear theory impact point estimator. The impact errors asymptotically approach zero as the projectile approaches impact.

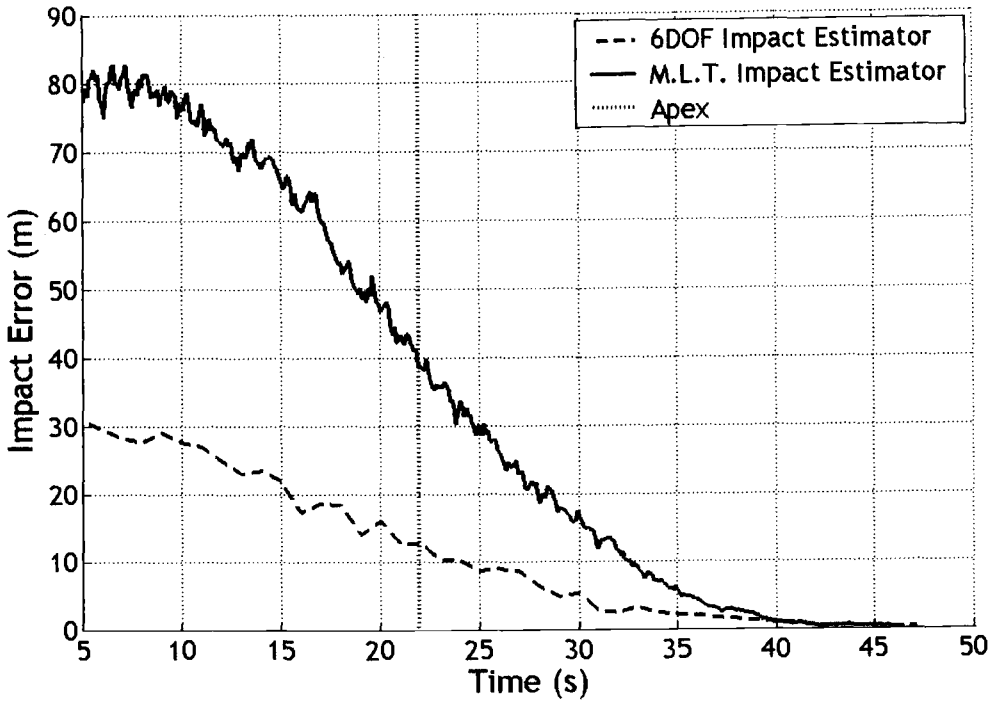

Figure 2.16: Impact Point Error versus Time for 12 State Filter

Figure 2.17 shows predicted ground impact point as the projectile moves through its trajectory for a single six degree of freedom impact point estimation. The impact points reported in this figure occur at a data rate of 1 Hz. The majority of the impact point estimation error is in the downrange distance, with the cross range error generally being less than 5 m.

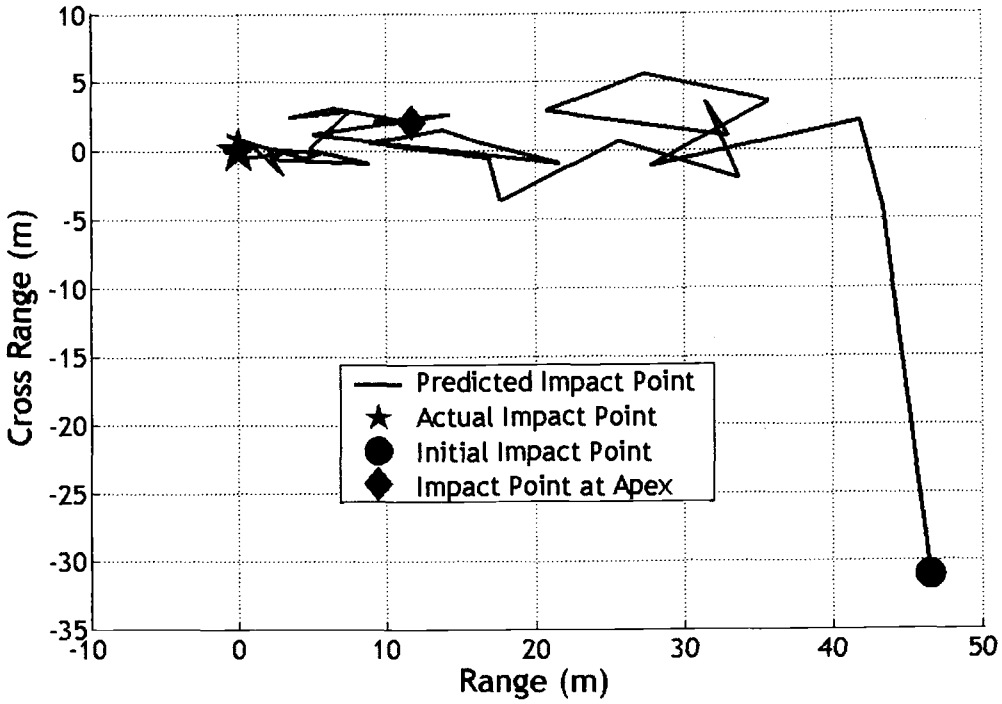

Figure 2.17: Ground Impact Point Predicted By 12 State Filter and 6 DOF Estimator

Position, Velocity, and Angular Velocity Measurement

The measurement model used in this simulation assumes that nine measurements (x, y, z, $\dot{x}$, $\dot{y}$, $\dot{z}$, $\tilde{p}$, $\tilde{q}$, $\tilde{r}$) are available, corresponding to the measurements available with a sensor combination consisting of G.P.S. and rate gyros. The 100 Hz measurements have simulated Gaussian noise superimposed as detailed in Table 1.

Figure 2.18 shows magnitude of impact point error as a function of time as computed by both the six degree of freedom and the modified linear theory impact point estimators. Each error line is the average of ten simulations. At the apex of the trajectory the predicted impact point has an error of 50 m for the six degree of freedom impact point estimator and 100 m for the modified linear theory impact

point estimator. As the projectile approaches impact, the impact errors linearly approach zero.

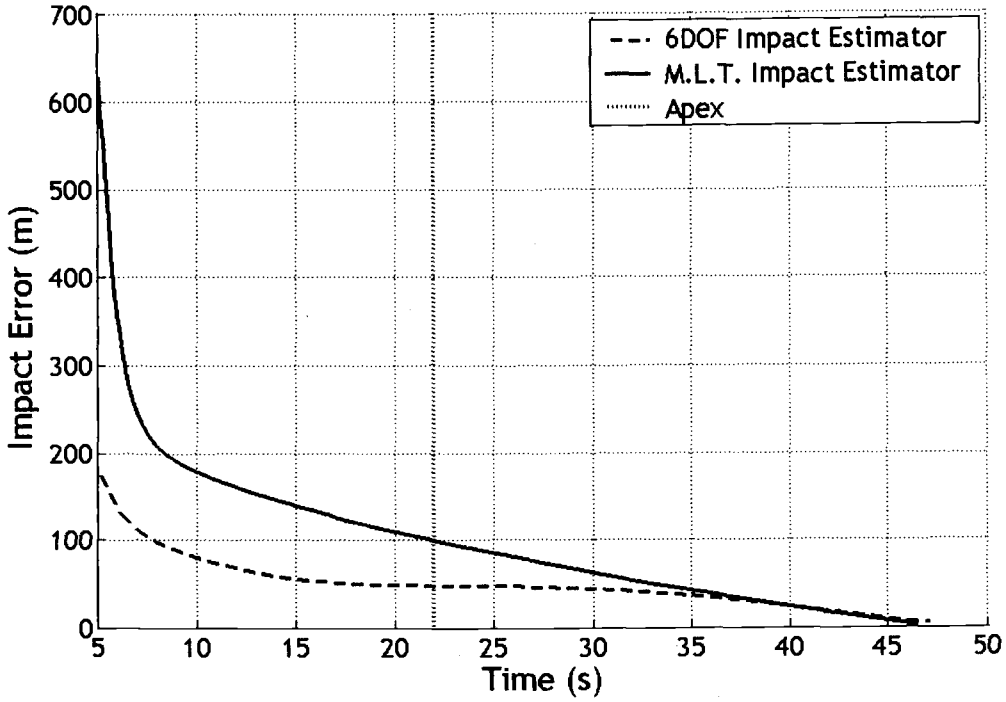

Figure 2.18: Impact Point Error versus Time for 9 Measurement Filter

Position, Velocity, Roll, and Roll Rate Measurement

The measurement model used in this simulation assumes that eight measurements (x, y, z, $\dot{x}$, $\dot{y}$, $\dot{z}$, ϕ, $\dot{\phi}$) are available, corresponding to the measurements available with a sensor combination consisting of G.P.S. and a magnetometer. The 100 Hz measurements have simulated Gaussian noise superimposed as detailed in Table 1.

Figure 2.19 shows the magnitude of the error in predicted impact point as a function of time as computed by both the six degree of freedom and the modified linear theory impact point estimators. Each error line is the average of ten

simulations. At the apex of the trajectory the predicted impact point has an error of 10 m for the six degree of freedom impact point estimator and less than 65 m for the modified linear theory impact point estimator. At the apex, the impact point error predicted by the six degree of freedom propagator is increasing to a maximum of 23 m at 15 seconds to impact. From that point the six degree of freedom model begins to approach zero impact error. The modified linear theory impact point error shows a linear trend towards zero impact error as the projectile approaches the impact point.

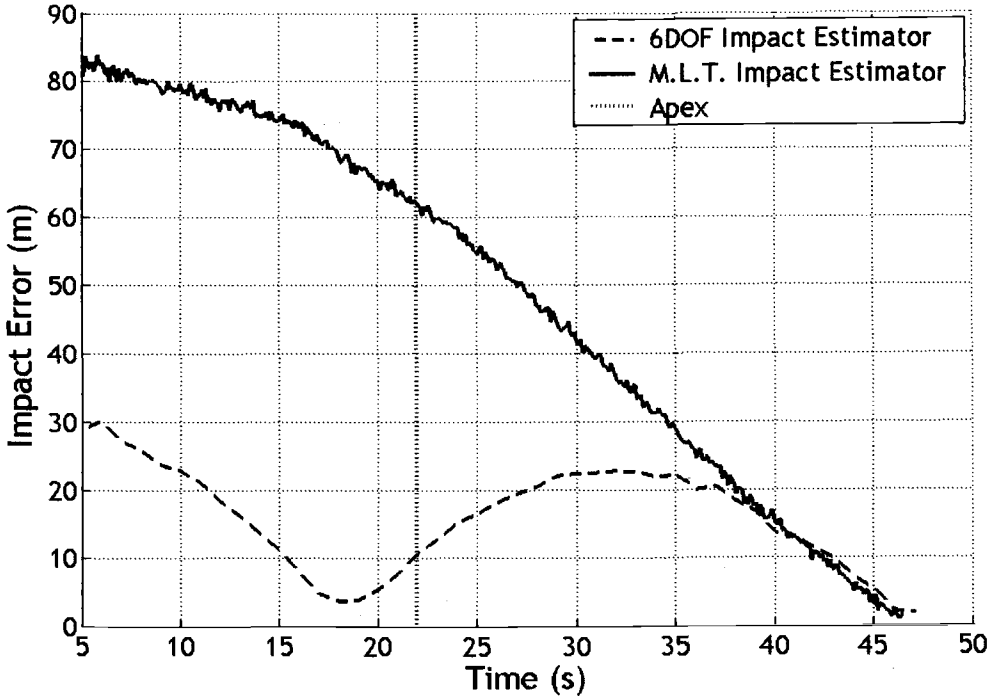

Figure 2.19: Impact Point Error versus Time for 8 Measurement Filter

CONCLUSION

The combination of modified projectile linear theory and Kalman filtering reported here can successfully predict the impact point of a projectile in flight.

Predicted impact point error at the apex of flight for an indirect fire trajectory is sufficiently small to warrant implementation into model predictive control algorithms or automatic round registration systems. Effective implementation of an in flight impact point estimation routine requires that the routine process quickly and efficiently providing estimations to a projectile control system in a timely manner while not overburdening the on round processor. The algorithm using numerical simulation of a fully non-linear dynamic model for propagation to the target requires significant on board processing power whereas the modified projectile linear theory propagator can be easily implemented into a real time computer system.

Impact point estimation error is fairly evenly divided between state estimation error and propagation error, except in the case when position, velocity, and roll measurements are available. In this case, the impact point estimation error is predominately comprised of model propagation errors earlier in flight and state estimation errors as the projectile approaches impact. Impact point estimation error also tends to occur more predominately in the down range direction, with cross range error becoming reasonably small early in flight.

REFERENCES

1. Merhav, S., "Aerospace Sensor Systems and Applications," Springer-Verlag New York, Inc., New York, 1996.

2. Aldrich, G., W. Krabill, "A Versatile Kalman Technique for Aircraft or Missile State Estimation and Error Analysis using Radar Tracking Data," AIAA Guidance and Control Conference, Stanford, CA, Paper No. AIAA-72-838, 1972.

3. Widall, W., "Enlarging the Region of Convergence of Kalman Filters that Encounter Nonlinear Elongation of Measured Range," AIAA Guidance and Control Conference, Stanford, CA, Paper No. AIAA-72-879, 1972.

4. Speyer, J., D. Hull, "Comparison of Several Extended Kalman Filter Formulations for Homing Missile Guidance," AIAA Guidance and Control Conference, Danvers, Mass., Paper No. AIAA-80-1786, 1980.

5. Chin, H., "Distributed Kalman Filter in an Integrated SAHRS/GPS Navigation System," Guidance, Navigation, and Control Conference, Snowmass, CO, Paper No. AIAA-85-1878, 1985.

6. Lam, Q., P. Pal, R. Welch, W. Grossman, "Magnetometer Based Attitude Determination System using a Reduced Kalman Filter," AIAA/AAS Astrodynamics Conference, San Diego, CA, Paper No. AIAA-96-3629, 1996.

7. Burchett, B., M. Costello, "Specialized Kalman Filtering for Guided Projectiles," 39th AIAA Aerospace Sciences Meeting and Exhibit, Reno, NV, Paper No. AIAA-2001-1120, 2001.

8. Shkolnikov, I., Y. Shtessel, P. Zarchan, D. Lianos, "Simulation Study of the Homing Interceptor Guidance Loop with Sliding Mode Observers versus

Kalman Filter," AIAA Guidance, Navigation, and Control Conference and Exhibit, Montreal, Canada, Paper No. AIAA-2001-4216

9. Kalman, R. E., "A New Approach to Linear Filtering and Prediction Problems," *Transactions of the ASME-Journal of Basic Engineering*, 82, 34-45, 1960.
10. Stengel, R., "Optimal Control and Estimations," Dover Publications, Inc., New York, 1994.
11. Costello, M., D. Anderson, "M. Costello, D. Anderson, "Effect of Internal Mass Unbalance on the Terminal Accuracy and Stability of a Projectile," AIAA Paper Number 96-3447, Proceedings of the 1996 AIAA Flight Mechanics Conference, San Diego, CA, 1996.
12. Hainz, L., M. Costello, "Modified Linear Theory for Rapid Trajectory Prediction," *Journal of Guidance, Control, and Dynamics*, Currently in review, 2004.

GENERAL CONCLUSION

The two papers forming this thesis combine to provide a complete impact point estimation algorithm. The first paper proposes a modified projectile linear theory which can be used to propagate the state of a projectile forward in time with reasonable accuracy. The second paper proposes a complete impact point estimation algorithm which can effectively predict the impact point of an indirect fire projectile.

The modified projectile linear theory model provides a reasonably accurate and relatively simple model of the dynamics of a projectile in flight capable of handling high pitch angles. The closed form solutions of modified linear theory can be used to propagate the projectile state forward in time without the need for excessive computational power. The modified projectile linear theory model provides a linear model of projectile dynamics that can be used to evaluate projectile stability or design linear projectile control laws.

The combination of modified projectile linear theory and Kalman filtering reported in the second paper successfully predicts the impact point of a projectile in flight. Predicted impact point error at the apex of flight for an indirect fire trajectory is sufficiently small to warrant implementation into model predictive control algorithms or automatic round registration systems. Effective implementation of an in flight impact point estimation routine requires that the routine process quickly and efficiently providing estimations to a projectile control system in a timely manner while not overburdening the on round processor. The algorithm using numerical simulation of a fully non-linear dynamic model for propagation to the target requires

significant on board processing power whereas the modified projectile linear theory propagator can be easily implemented into a real time computer system.

The Kalman filter is able to estimate the projectile state with reasonable accuracy even when confronted noisy and partial state measurements. Although the filter is most accurate when full state measurements are provided, it has ability to form a reasonably accurate state estimation from noisy partial state measurements. This allows a projectile control system to operate with fewer and less accurate sensors.

BIBLIOGRAPHY

Aldrich, G., W. Krabill, "A Versatile Kalman Technique for Aircraft or Missile State Estimation and Error Analysis using Radar Tracking Data," AIAA Guidance and Control Conference, Stanford, CA, Paper No. AIAA-72-838, 1972.

Burchett, B., M. Costello, "Specialized Kalman Filtering for Guided Projectiles," 39th AIAA Aerospace Sciences Meeting and Exhibit, Reno, NV, Paper No. AIAA-2001-1120, 2001.

Burchett, B., A. Peterson, M. Costello, "Prediction of Swerving Motion of a Dual-Spin Projectile with Lateral Pulse Jets in Atmospheric Flight," *Mathematical and Computer Modeling*, Vol. 35, No. 1-2, pp. 1-14, 2002.

Burchett, B., M. Costello, "Model Predictive Lateral Pulse Jet Control of an Atmospheric Rocket," *Journal of Guidance, Control, and Dynamics*, Vol 25, No 5, pp 860-867, 2002.

Chin, H., "Distributed Kalman Filter in an Integrated SAHRS/GPS Navigation System," Guidance, Navigation, and Control Conference, Snowmass, CO, Paper No. AIAA-85-1878, 1985.

Cobb, K., R. Whyte, P. Laird, "Effects of a Moving Components on the Motion of a 20-mm Projectile," 11th AIAA Aerodynamics Testing Conference, Mar 18-20, Colorado Springs, CO, USA, pp. 94-103, 1983.

Cooper, G., "Influence of Yaw Cards on the Yaw Growth of Spin Stabilized Projectiles," *Journal of Aircraft*, Vol. 38, No. 2, pp. 266-270, 2001.

Costello, M., D. Anderson, "M. Costello, D. Anderson, "Effect of Internal Mass Unbalance on the Terminal Accuracy and Stability of a Projectile," AIAA Paper Number 96-3447, Proceedings of the 1996 AIAA Flight Mechanics Conference, San Diego, CA, 1996.

Costello, M., A. Peterson, "Linear Theory of a Dual-Spin Projectile in Atmospheric Flight, *Journal of Guidance, Control, and Dynamics*, Vol. 23, No. 5, pp. 789-797, 2000.

Fowler, R., E. Gallop, C. Lock, H. Richmond, "The Aerodynamics of a Spinning Shell," *Philosophical Transactions of the Royal Society of London*, Series A, Vol 221, 1920.

Guidos, B., G. Cooper, "Closed Form Solution of Finned Projectile Motion Subjected to a Simple In-Flight Lateral Impulse," 38th AIAA Aerospace Sciences Meeting and Exhibit, Reno, NV, Paper No. AIAA-2000-0767, 2000.

Hainz, L., M. Costello, "Modified Linear Theory for Rapid Trajectory Prediction," *Journal of Guidance, Control, and Dynamics*, Currently in review, 2004.

Hodapp, A., "Effect of Mass Asymmetry on Ballistic Match of Projectiles," *Journal of Spacecraft and Rockets*, Vol. 13, No. 12, pp. 757-760, 1976.

Hodapp, A., "Passive Means for Stabilizing Projectiles with Partially Restrained Internal Members", *Journal of Guidance, Control, and Dynamics*, Vol. 12, No. 2, pp. 135-139, 1989.

Kalman, R. E., "A New Approach to Linear Filtering and Prediction Problems," *Transactions of the ASME-Journal of Basic Engineering*, 82, 34-45, 1960.

Kelley, J., E. McShane, "On the Motion of a Projectile with Small or Slowly Changing Yaw," Ballistic Research Laboratory Report 446, Aberdeen Proving Ground, MD, 1944.

Kelley, J., E. McShane, F. Reno, "Exterior Ballistics", University of Denver Press, 1953.

Kent, R., "An Elementary Treatment of the Motion of a Spinning Projectile About its Center of Gravity," Ballistic Research Laboratory Report 85, Aberdeen Proving Ground, MD, 1937.

Lam, Q., P. Pal, R. Welch, W. Grossman, "Magnetometer Based Attitude Determination System using a Reduced Kalman Filter," AIAA/AAS Astrodynamics Conference, San Diego, CA, Paper No. AIAA-96-3629, 1996.

McCoy, R., "Modern Exterior Ballistics", Schiffer Publishing Ltd., Attlen, PA, pp 165-183 & 240-244, 1999.

Merhav, S., "Aerospace Sensor Systems and Applications," Springer-Verlag New York, Inc., New York, 1996.

Murphy, C., "Angular Motion of a Spinning Projectile with a Viscous Liquid Payload," *Journal of Guidance, Control, and Dynamics,* Vol. 6, No. 4, pp. 280-286, 1983.

Murphy, C., "Instability of Controlled Projectiles in Ascending or Descending Flight," *Journal of Guidance and Control*, Vol. 4, No. 1, pp. 66-69, 1981.

Nielson, K., J. Synge, "On the Motion of a Spinning Shell," Ballistic Research Laboratory Report 116, Aberdeen Proving Ground, MD, 1943.

Shkolnikov, I., Y. Shtessel, P. Zarchan, D. Lianos, "Simulation Study of the Homing Interceptor Guidance Loop with Sliding Mode Observers versus Kalman Filter," AIAA Guidance, Navigation, and Control Conference and Exhibit, Montreal, Canada, Paper No. AIAA-2001-4216

Soper, W., "Projectile Instability Produced by Internal Friction," AIAA Journal, Vol. 16, No. 1, pp. 8-11, 1978.

Speyer, J., D. Hull, "Comparison of Several Extended Kalman Filter Formulations for Homing Missile Guidance," AIAA Guidance and Control Conference, Danvers, Mass., Paper No. AIAA-80-1786, 1980.

Stengel, R., "Optimal Control and Estimations," Dover Publications, Inc., New York, 1994.

Weber, D., "Simplified Method for Evaluating the Flight Stability of Liquid-Filled Projectiles," *Journal of Spacecraft and Rockets*, Vol. 31, No. 1, pp. 130-134, 1994.

Widall, W., "Enlarging the Region of Convergence of Kalman Filters that Encounter Nonlinear Elongation of Measured Range," AIAA Guidance and Control Conference, Stanford, CA, Paper No. AIAA-72-879, 1972.